UPPSALA
UNIVERSITET

UPTEC W 21032
Examensarbete 30 hp
Juni 2021

Precipitation variability modulates the terrestrial carbon cycle in Scandinavia

Ella Ek

Abstract

Precipitation variability modulates the terrestrial carbon cycle in Scandinavia
Ella Ek

Climate variability and the carbon cycle (C-cycle) are tied together in complex feedback loops and due to these complexities there are still knowledge-gaps of this coupling. However, to make accurate predictions of future climate, profound understanding of the C-cycle and climate variability is essential. To gain more knowledge of climate variability, the study aims to identify recurring spatial patterns of the variability of precipitation anomalies over Scandinavia during spring and summer respectively between 1981 to 2014. These patterns will be related to the C-cycle through changes in summer vegetation greenness, measured as normalized difference vegetation index (NDVI). Finally, the correlation between the patterns of precipitation variability in summer and the teleconnection patterns over the North Atlantic will be investigated.

The precipitation data was obtained from ERA5 from the European Centre for Medium-Range Weather Forecasts and the patterns of variability were found through empirical orthogonal function (EOF) analysis. The first three EOFs of the spring and the summer precipitation anomalies together explained 73.5 % and 65.5 % of the variance respectively. The patterns of precipitation variability bore apparent similarities when comparing the spring and summer patterns and the Scandes were identified to be important for the precipitation variability in Scandinavia during both seasons.

Anomalous events of the spring EOFs indicated that spring precipitation variability had little impact on anomalies of summer NDVI. Contradictory, summer precipitation variability seemed to impact anomalies of summer NDVI in central- and northeastern Scandinavia, thus indicating that summer precipitation variability modulates some of the terrestrial C-cycle in these regions. Correlations were found between a large part of the summer precipitation variability and the Summer North Atlantic Oscillation and the East Atlantic pattern. Hence, there is a possibility these teleconnections have some impact, through the summer precipitation variability, on the terrestrial C-cycle.

Keywords: Terrestrial carbon cycle, NDVI, Precipitation variability, EOF analysis, Scandinavia.

Department of Earth Sciences, Program for Air, Water and Landscape Science, Uppsala University, Villavägen 16, SE-75236 Uppsala, Sweden.

Referat

Variation i nederbörd styr den terrestra kolcyckeln i Skandinavien
Ella Ek

Förändringar och variation i klimatet är sammankopplade med kolcykeln genom komplexa återkopplingsmekanismer. På grund av denna komplexitet är kunskapen om kopplingen mellan klimatvariation och kolcykeln fortfarande bristande, men för att möjliggöra precisa prognoser om framtida klimat är det viktigt att ha kunskap om denna koppling. För att få mer kunskap om klimatvariation syftar därför denna studie till att identifiera återkommande strukturer av nederbördsvariation över Skandinavien under vår respektive sommar från 1981 till 2014. Dessa relateras till förändringar i sommarväxtlighetens grönhet, uppmätt som skillnaden i normaliserat vegetationsindex (NDVI). Även korrelationen mellan sommarstrukturerna av nederbördsvariationen och storskaliga atmosfäriska svängningar, s.k. "teleconnections", över Nordatlanten undersöks.

Nederbördsdatan erhölls från ERA5 analysdata från Europacentret för Medellånga Väderprognoser och strukturer av nederbördsvariationen identifierades genom empirisk ortogonal funktionsanalys (EOF) av nederbördsavvikelser. De tre första EOF av vår- respektive sommarnederbördsavvikelser förklarade tillsammans 73,5 % respektive 65,5 % av nederbördsvariationen. Strukturerna av nederbördsvariation under vår respektive sommar uppvisade tydliga likheter sinsemellan. Dessutom identifierades Skanderna vara av stor vikt för nederbördsvariationen i Skandinavien under båda årstider.

Avvikande år av nederbördsvariation under våren indikerade att sagda nederbördsvariation haft liten påverkan på NDVI-avvikelser under sommaren. Emellertid verkade nederbördsvariationen under sommaren påverkat NDVI-avvikelser under sommaren i centrala och nordöstra Skandinavien. Detta indikerar att nederbördsvariationen under sommaren till viss del styr den terrestra kolcykeln i dessa regioner. För nederbördsvariationen under sommaren fanns korrelation mellan både Nordatlantiska sommaroscillationen och Östatlantiska svängningen. Det finns således en möjlighet att dessa "teleconnections" har en viss påverkan på den terrestra kolcykeln genom nederbördsvariationen under sommaren.

Nyckelord: Terrestra kolcykeln, NDVI, Nederbördsvariation, EOF analys, Skandinavien.

Institutionen för geovetenskaper, Luft-, vatten- och landskapslära, Uppsala Universitet, Villavägen 16, 75236 Uppsala, Sweden.

Preface

This thesis, holding 30 credits, concludes my five year long studies at the Master's Programme in Environmental and Water Engineering at Uppsala University and the Swedish University of Agricultural Sciences (SLU). Supervisor was Gabriele Messori, Senior lecturer/Associate Professor at the Department of Earth Sciences, Program for Air, Water and Landscape Sciences; Meteorology. Subject reader was Minchao Wu, Postdoctoral position at the same department.

I want to wholeheartedly thank my supervisor and subject reader Gabriele Messori and Minchao Wu for all their support, engagement and encouragement throughout the project. Your ideas and fast answers to every single question I have had have been most appreciated and very valuable to me.

As my studies in Uppsala come to an end I would also like to take the opportunity to thank my friends for advice and an unforgettable time. It would not have been possible for me to complete my studies without the love and support from my family and for this I want to thank them as well. The final thank goes to Albin Leding, stuck at the home office with me during the entire semester. I am most grateful for your patience and our discussions.

Ella Ek
Uppsala, 2021.

UPTEC W 21032, ISSN 1401–5765
Published digitally in DiVA, 2021, by the Department of Earth Sciences, Uppsala University. (http://www.diva-portal.org/)

Populärvetenskaplig sammanfattning

Kol är ett grundämne som finns överallt på jorden och som flödar mellan atmosfär, hav, land, berggrund samt växt- och djurliv. Flödet mellan dessa delar brukar kallas för kolcykeln, och om det sker en förändring i någon del av kolcykeln kommer alla andra delar också att påverkas. I förlängningen kommer detta även att ha inverkan på vårt klimat. Samtidigt kan också variationer i klimatet påverka kolcykeln. Samverkan mellan kolcykeln och variationer i klimatet är alltså mycket komplicerad och det finns fortfarande stora kunskapsluckor som behöver fyllas om hur denna samverkan går till för att kunna göra mer noggranna förutsägelser om jordens framtida klimat. Detta gäller speciellt eftersom jorden oftare kommer utsättas för mer extrema väderförhållanden i takt med att den värms upp. Sådana extrema väderförhållanden kan exempelvis innebära ovanlig torka eller ovanligt kraftig nederbörd, vilket påverkar vegetationen och därigenom även kolcykeln.

I denna studie undersöks om det finns återkommande mönster för variabiliteten av nederbördsavvikelser under vår och sommar i Skandinavien mellan åren 1981 till 2014. Detta kopplas till kolcykeln genom att undersöka om nederbördsavvikelser påverkat avvikelser i sommarvegetationen i Skandinavien under samma period. Dessutom undersöks om det finns en koppling mellan de återkommande mönstren av nederbördsavvikelser och variation i klimatet över Nordatlanten, som beskrivs av storskaliga atmosfäriska mönster.

Med hjälp av satelliter kan aktiviteten av vegetation mätas, vilket ger en uppskattning av växtlighetens del av kolcykeln. Avvikelser i växtlighetens kolcykel uppskattades därför genom att beräkna avvikelser av sommarvegetationens aktivitet.

Under såväl vår som sommar identifierades tre stycken framträdande och återkommande mönster för variabiliteten av nederbördsavvikelser. De tre mönster som framträdde för våren förklarade tillsammans 73,5 % av variabiliteten. Under sommaren förklarade de tre framträdande mönstren tillsammans 65,5 % av variabiliteten. De tre framträdande mönstren hade liknande utseende under våren som under sommaren. Det var även tydligt att den Skandinaviska fjällkedjan var viktig för variabiliteten av nederbördsavvikelser under både vår och sommar eftersom fjällkedjan framträdde tydligt i mönstren.

Vegetationsaktiviteten undersöktes sedan under vissa utvalda år av extrem variabilitet av nederbördsavvikelser. Från detta drogs slutsatsen att nederbördsavvikelser under våren inte haft så stor inverkan på aktiviteten av sommarvegetationen. Däremot verkade nederbördsavvikelser under sommaren haft viss inverkan på aktiviteten av sommarvegetationen i centrala och nordöstra Skandinavien. Detta tyder alltså på att nederbördsavvikelser under sommaren till viss del även har påverkat växtlighetens kolcykel under sommaren.

Slutligen identifierades även en koppling mellan en stor del av nederbördsavvikelser under sommaren och två av de storskaliga atmosfäriska mönstren, nämligen den Nordatlantiska Sommaroscillationen och den Östatlantiska svängningen. Detta innebär att nederbördsavvikelser under sommaren till viss del har styrts av dessa två storskaliga atmosfäriska mönster. Detta i sin tur indikerar att dessa storskaliga atmosfäriska mönster även styr växtlighetens kolcykel i centrala och nordöstra Skandinavien.

Contents

1 Abbreviations

- **AL:** Atlantic Low, one of four weather regimes identified over the North Atlantic region during summer
- **AR:** Atlantic Ridge, one of four weather regimes identified over the North Atlantic region during summer
- **C-cycle:** carbon cycle, the complex flows of carbon between the different components of the Earth system
- **EA:** East Atlantic pattern, a teleconnection pattern identified over the North Atlantic region
- **EOF:** empirical orthogonal function, a mathematical analysis concept possible to use for identifying spatial patterns of variability
- **ERA5:** the fifth generation of reanalysis data from the European Centre for Medium-Range Weather Forecasts
- **GPP:** gross primary production, the amount of CO_2 sequestered by terrestrial ecosystems through photosynthesis
- **LUE:** light use efficiency of plants
- **NDVI:** normalized difference vegetation index, an index for vegetation greenness that gives a measure of the photosynthetically active biomass of vegetation
- **NIR:** near-infrared
- **NAO:** North Atlantic Oscillation, one of four weather regimes identified over the North Atlantic region during winter. Also defined as a teleconnection pattern
- **NPP:** net primary production, the sum of plant respiration and plant net gain of carbon
- **PC:** principal component, associated time series to the spatial variability pattern of an EOF
- **REOF:** rotated empirical orthogonal function
- **SBL:** Scandinavian Blocking, one of four weather regimes identified over the North Atlantic region during winter
- **SCA:** Scandinavian pattern, a teleconnection pattern identified over the North Atlantic region
- **SLP:** sea-level pressure
- **SNAO:** Summer North Atlantic Oscillation, one of four weather regimes identified over the North Atlantic region during summer
- **VIS:** visible spectrum

2 Introduction, objective and aim

As the Earth's climate is changing due to anthropogenic activities and as extreme weathers become more common (Ciais et al. 2013; Seneviratne et al. 2012), it is important to have a profound understanding of the processes governing the Earth system and how these will be affected by variations of the climate. The global carbon cycle (C-cycle), and by extension the terrestrial C-cycle, control processes such as atmospheric composition and vegetation activity, thus affecting the complex flows of carbon between the different components of the Earth system. As the amount of CO_2 increases in the atmosphere due to anthropogenic forcing, the carbon fluxes will be affected (Ciais et al. 2013; NASA 2011). In general, climate variability impacts the terrestrial C-cycle, thus creating complex feedback loops. Because of these complexities there are still knowledge-gaps of the coupling between the C-cycle and climate variability (Messori et al. 2019; Piao et al. 2019).

Plants and soil micro-organisms within the terrestrial biosphere intuitively benefit from higher temperatures, larger insolation and greater water availability (Chapin et al. 2011). However, water availability and solar radiation are often negatively correlated as more precipitation typically corresponds to a more extensive cloud cover. Moreover, the limiting resources for productivity are highly variable on Earth (Churkina & Running 1998; Nemani et al. 2003). As the activity of the terrestrial C-cycle is problematic to measure, it has often been estimated through surface greenness (Myneni et al. 1997).

The interactions of the C-cycle and climate have been investigated for single variables, e.g. precipitation, as well as for entire climate modes of variability. However, the correlation between such climate modes in the North Atlantic region and the C-cycle has been found to vary between studies (Messori et al. 2019). Hence, in order to gain more understanding of the interactions between the terrestrial C-cycle and climate variability, and to be able to make accurate predictions of future climate and well-informed management decisions, the present study aims to identify patterns of precipitation variability and investigate their relation to the terrestrial C-cycle. The focus area of the study is Scandinavia.

The aim of the present study is to identify robust, recurring precipitation patterns over Scandinavia and relate these to changes in surface greenness over the region during the 34 year period of 1981 to 2014. The aim will be achieved by answering the following research questions, where "spring" equals the months March, April and May and "summer" June, July and August.

i. Which large scale spatial patterns explain the precipitation variability over Scandinavia in spring and summer respectively between 1981 to 2014?

ii. What are the roles of spring precipitation variability in affecting summer vegetation greenness in Scandinavia?

iii. What are the roles of summer precipitation variability in affecting summer vegetation greenness in Scandinavia?

iv. Is there a relation between the summer precipitation patterns and teleconnection patterns in the North Atlantic region?

3 Theory

3.1 Carbon cycle

One of the major chemical elements composing the Earth is carbon and it continuously exchanges between the different components of the Earth System: the atmosphere, the oceans, the land, the biosphere and the lithosphere (Fig. 1). These complex fluxes of carbon are referred to as the C-cycle (Ciais et al. 2013). The C-cycle occurs at different temporal and spatial scales, including processes such as the carbon exchanges through the stomata of a leaf within seconds or the formation of permafrost during hundreds of thousands of years (NASA 2011). Large-scale effects can thus be imposed on the climate system due to a changed C-cycle, through changes in the features of biogeochemical or biogeophysical processes. Such changes could be within the atmospheric composition or land surface properties, which modulate radiative forcing and feedbacks in the Earth system (Ciais et al. 2013; Chapin et al. 2011). Simultaneously, the variability of climate and its extremes can highly affect the C-cycle and so the C-cycle and climate create complex feedback loops as they impact each other (Messori et al. 2019; Reichstein et al. 2013).

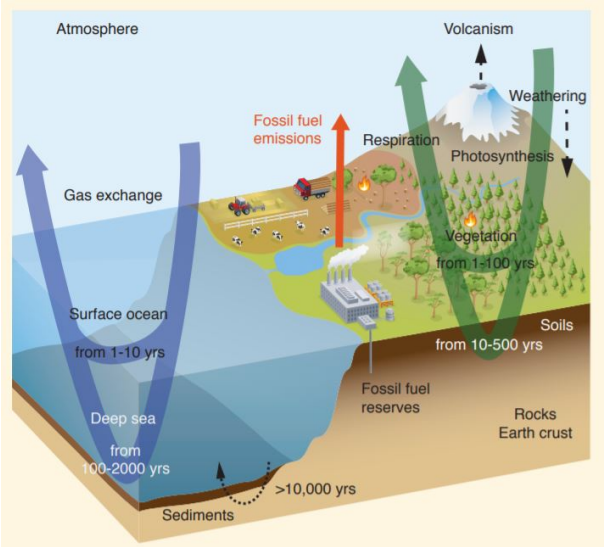

Figure 1: Simplified schematic of the global carbon cycle showing the typical turnover time scales for carbon transfers through the major reservoirs. Figure and caption according to Ciais et al. (2013), FAQ 6.2 Figure 1 (p. 544). Reproduced according to IPCC copyright.

3.1.1 Terrestrial carbon cycle

The terrestrial C-cycle is a major domain of the C-cycle, where carbon is stored in vegetation, soil, wetland and permafrost. The carbon fluxes within the terrestrial C-cycle encompass several important, complicated ecosystem processes at different scales, such as decomposition, respiration and photosynthesis (Ciais et al. 2013).

At the scales of ecosystems and individual trees, the terrestrial biosphere absorbs CO_2 through the photosynthesis of vegetation, during which carbon is assimilated through the utilization of nutrients, water and photosynthetic active radiation, i.e. the specific

spectrum of radiation available for vegetation. Depending on the accessibility of these three resources, the photosynthesis rate varies diurnally, seasonally and yearly (Chapin et al. 2011).

The small-scale processes are of importance for changes in the C-cycle. The visible light reaching a leaf on a plant is absorbed by the pigment chlorophyll within the leaf cells. However, the sun's angle, cloud cover, sunflecks and the distribution of leaf area in the canopy can have a major impact on the availability of incident light. To adapt to this, plants can adjust the leaf angle to retain effective photosynthesis according to the prevailing conditions. Another important process is adjustment of the stomata, which regulates the absorption of CO_2 by diffusion into the leafs. Hence, there is an optimized balance between the water use and available radiation or CO_2 uptake in response to changing environmental conditions. In general, vegetation has the ability to physically adjust to the prevailing conditions to maintain an efficient photosynthesis (Chapin et al. 2011).

The productivity of vegetation, measured as the photosynthesis performed, is clearly affected by variations of climate-controlled growing conditions and according to Churkina & Running (1998) there are usually several climatic factors affecting the primary productivity of ecosystems. Gross primary production (GPP) is a common and useful metric to reflect the carbon uptake of ecosystems, defined as the amount of CO_2 sequestered by terrestrial ecosystems through photosynthesis. Another metric is net primary production (NPP) which is the sum of plant respiration and plant net gain of carbon. Variability of GPP can occur due to changes in light, temperature and water- and nutrient availability combined with the effects of soil status. Sensitivities to these factors are usually different for vegetation types, climate and perturbations (Chapin et al. 2011).

3.1.2 Normalized difference vegetation index (NDVI)

Satellite-based measurements are efficient approaches to estimate ecosystem productivity such as NPP or GPP (Chapin et al. 2011). Such satellite-based measurements are often used as equivalents of primary production since other measures of productivity, e.g. NPP and GPP, are very complex to measure at large spatial scales (Myneni et al. 1997; Ågren & Andersson 2012). Such satellite-based measurements rely on the empirical relationship between light use efficiency (LUE) and radiation reflectance (Chapin et al. 2011). The underlying mechanism is that chlorophylls are efficient at spectral absorption in the visible spectrum (VIS) and the cellular structure of leaves causes the leaves to be highly reflective for the near-infrared (NIR) light spectrum. Thus, vegetation is effective at absorbing and reflecting light in different spectrums than other surfaces. Due to these specific properties, it is possible to calculate an index for vegetation greenness, denoted as the normalized difference vegetation index (NDVI) (Eq. 1). NDVI can provide a quantitative measure of the spatial and temporal variability of the photosynthetically active biomass of vegetation and has often been used as approximations of the activity of the terrestrial C-cycle (Myneni et al. 1997; Tucker 1979).

$$NDVI = \frac{NIR - VIS}{NIR + VIS} \tag{1}$$

Generally, ecosystems with high carbon uptake have a large content of chlorophyll that

absorbs the majority of incoming VIS and extensive leaf area which reflects a significant part of NIR, leading to green vegetation and a high NDVI according to Eq. 1 (Chapin et al. 2011). Additionally, NDVI has in some cases been found to have an exponential correlation with GPP (Wang et al. 2004). It is important to note, however, that different species might have different cellular leaf structures causing differences in reflected NIR, subsequently resulting in differences of NDVI. One should therefore be cautious when comparing NDVI for considerably different ecosystems and also bear in mind the possible contamination by the reflectance from other surface objects, e.g. background soil (Chapin et al. 2011). The value of NDVI theoretically lies between -1.0 to 1.0, where bare soil often ranges between -0.1 to 0.1 whereas clouds, water and snow have negative values due to their spectral properties (Defries & Townshend 1994; Goward et al. 1985).

3.2 Climate modes of variability

The variability of climate can be measured and quantified via considerably different approaches, from separate environmental variables to entire climate modes of variability. The latter refers to recurrent atmospheric modes of some oscillatory nature. A term used to describe some climate modes of variability is "teleconnection", namely the correlation between concurrent climate anomalies at remote geographical locations (Wallace & Gutzler 1981). Patterns of variability in the atmosphere can also be defined as weather regimes, referring to patterns in some large-scale atmospheric variable - often geopotential height - characterized by either recurrence, persistence or quasi stationarity. Different regimes are thus identified by certain patterns of the atmospheric variability, spatially and temporally (Michelangeli et al. 1995). Teleconnections and weather regimes are convenient measures of climate variability since the changes they induce in the regional climate affect several environmental variables, so their phases provide a summary of these variables (Messori et al. 2019). Well known teleconnections are for example the El Niño-Southern Oscillation (ENSO) (Rasmusson & Wallace 1983), the East Atlantic pattern (EA) (Barnston & Livezey 1987) and the North Atlantic Oscillation (NAO) (Hurrell 1995). The phases and behaviours of teleconnections are often given as numerical indices, which indicate the properties of the anomaly. The index of NAO is for example often defined as the difference in sea-level pressure (SLP) between Lisbon in Portugal and Stykkisholmur in Iceland (Hurrell 1995).

3.2.1 North Atlantic weather regimes and teleconnections

The climate in the North Atlantic region naturally possesses a high variability (Fabiano et al. 2020). However, the spatial patterns identified as corresponding to the majority of the atmospheric variability vary depending on the method used for identifying them. The two common methods cluster analysis and empirical orthogonal function (EOF) analysis often produce slightly different answers. The different answers are notable when comparing the results of e.g. Barnston & Livezey (1987) or Wibig (1999) with Hurrell & Deser (2010) or Vautard (1990). The rotated EOF (REOF) approach of Barnston & Livezey (1987) and Wibig (1999) identifies nine and five weather regime patterns over Europe respectively, while four patterns are identified by Hurrell & Deser (2010) and Vautard (1990) through their cluster approach.

Through the clustering approach, four distinctive patterns have been identified on 500

hPa and 700 hPa geopotential heights during winter over the North Atlantic and Europe, namely the positive phase of the NAO, the negative phase of the NAO, the Scandinavian Blocking (SBL) and the Atlantic Ridge (AR), as described below (Fig. 2) (Cassou 2008; Fabiano et al. 2020; Hurrell & Deser 2010; Vautard 1990). Fil & Dubus (2005) validated that these four weather regimes best represents the state of atmospheric pressure and its variability in winter through both cluster- and EOF analysis.

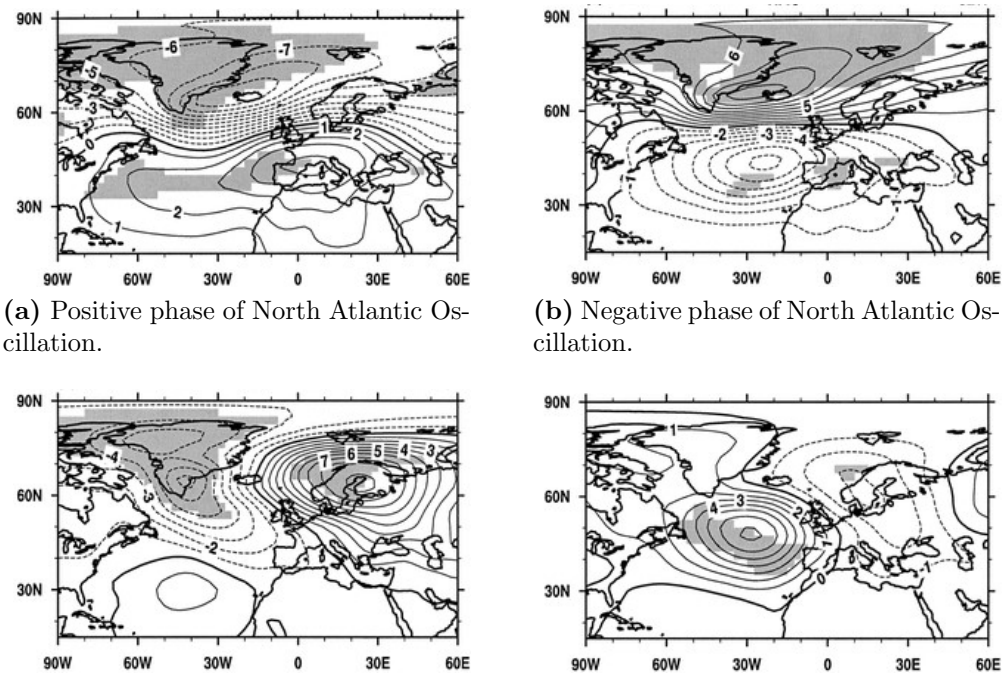

(a) Positive phase of North Atlantic Oscillation.

(b) Negative phase of North Atlantic Oscillation.

(c) Winter Scandinavian Blocking.

(d) Winter Atlantic Ridge.

Figure 2: Weather regimes in winter over the North Atlantic sector in 1949 to 2001. The regimes are defined through cluster analysis of average mean sea level pressure during December, January and February (Cassou et al. 2004). © **American Meteorological Society. Used with permission.**

The NAO is strongest during winter and is characterized by a SLP dipole, where the positive (negative) phase has a low (high) pressure anomaly center over Iceland and a high (low) pressure anomaly center over the Azores (Cassou 2008; Hurrell & Deser 2010). The characteristics of the SBL are strong blocking anticyclonic ridges over Scandinavia, hence this pattern is sometimes named solely "Blocking" (Fabiano et al. 2020; Hurrell & Deser 2010; Vautard 1990). SBL is sometimes named the Scandinavian pattern (SCA) (Fig. 3), a different name for a very similar atmospheric pattern (Cassou et al. 2004; Wang & Tang 2020, Wibig 1999). The AR pattern is recognized by anticyclonic ridges and

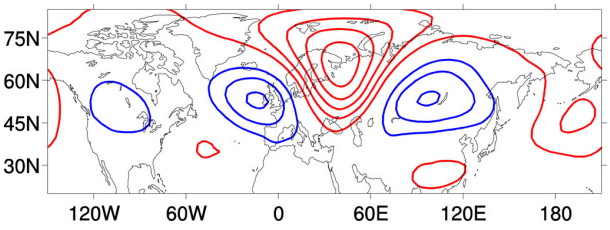

Figure 3: The pattern of SCA during December, January and February defined through REOF analysis of the mean 300 hPa geopotential height over Eurasia (Wang & Tan 2020). © **American Meteorological Society. Used with permission.**

high pressure anomalies, occurring approximately in the middle of the North Atlantic (Fabiano et al. 2020; Fil & Dubus 2005; Hurrell & Deser 2010). The AR-pattern has been found to bear a strong resemblance to the EA (Fig. 4), a pattern characterized by a dipole of pressure anomaly centers outside the European coast covering the North Atlantic from west to east (Barnston & Livezey 1987; Hurrell & Deser 2010; Moore et al. 2013; Wallace & Gutzler 1981).

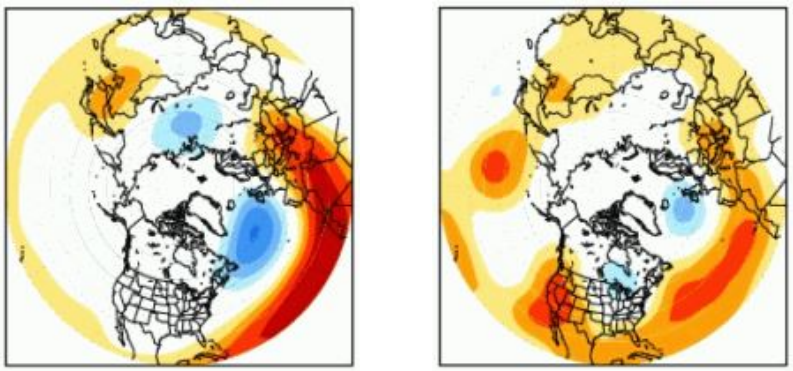

(a) Positive phase of the East Atlantic pattern in January.

(b) Positive phase of the East Atlantic pattern in July.

Figure 4: Positive phases of the East Atlantic pattern during January and July. Obtained from NOAA National Weather Service Climate Prediction Center (2005).

The weather regimes are still present and recurrent during summer, however not as persistently as during winter. An early study at 700 hPa geopotential height concluded through EOF analysis that five weather regimes could be identified over the North Atlantic region in summer which all bore resemblance to the winter weather regimes (Mukougawa & Sato 1999). In more recent studies, four patterns at 500 hPa geopotential height have been found and validated for summer over the North Atlantic region through cluster analysis (Fig. 5), namely the positive and negative phases of the NAO named the Summer North Atlantic Oscillation (SNAO), the Atlantic Low (AL) and the AR (Cassou et al. 2005; Folland et al. 2009; Guemas et al. 2010). The negative phase of the SNAO occurs as a dipole located between Greenland and northern Europe, the same pattern as during wintertime but with a smaller coverage and shifted centres, hence placed more northerly. AL has the clear characteristics of a deep trough over a vast area of the North Atlantic Ocean, in combination with much weaker pressure anomalies to the northwest covering Europe. A strong, anticyclonic anomaly over western Europe distinguishes the AR along with a low pressure anomaly to the northeast, extending from Scandinavia to Greenland (Cassou et al. 2005; Guemas et al. 2010). Moreover, Cassou et al. (2005) found that the summertime AL and AR patterns display resembling features to the teleconnection pattern EA. During the shoulder seasons, i.e. spring and autumn, very little work has been carried out regarding which weather regimes and teleconnections characterises these seasons due to the patterns not being well defined during spring and autumn (Atmospheric flow Analogues for Climate Change n.d.).

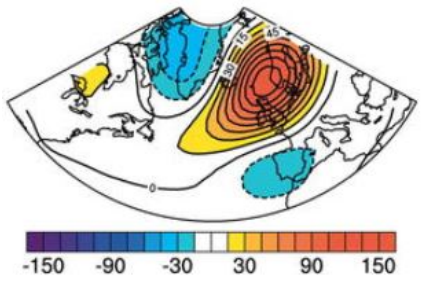

(a) Positive phase of Summer North Atlantic Oscillation.

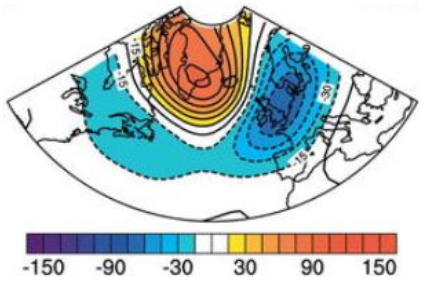

(b) Negative phase of Summer North Atlantic Oscillation.

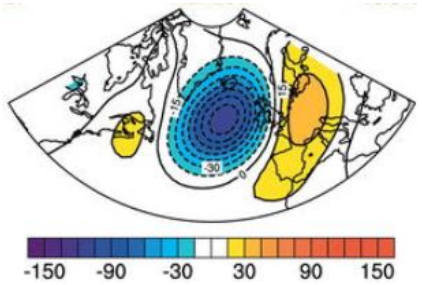

(c) Summer Atlantic Low.

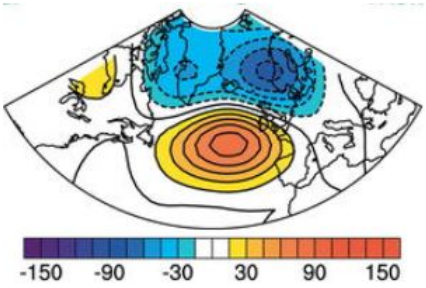

(d) Summer Atlantic Ridge.

Figure 5: Weather regimes in summer over North Atlantic and Europe in 1950 to 2003. The regimes are defined through cluster analysis at 500 hPa geopotential height (Cassou et al. 2005). © **American Meteorological Society. Used with permission.**

3.2.2 Precipitation in Europe

The modes of atmospheric variability over the North Atlantic have profound impact on several weather variables in Europe. For instance, according to Hurrell & Deser (2010), the index of the NAO "imply information about temperature, storms and precipitation, cloudiness, hydrographic characteristics, mixed-layer depths, and circulation patterns in the ocean".

The weather regimes and teleconnections in the North Atlantic sector thus influence precipitation over Europe and Wibig (1999) found through REOF analysis that during winter in Europe the NAO correlates strongly with precipitation over the British Isles, Scandinavia, Finland, France, Germany and Denmark. During time periods when NAO has a strong, positive phase, the region where the maximum moisture transport occurs changes and reaches further north, extending to Scandinavia (Hurrell 1995). Positive phases of the NAO thus leads to increased precipitation during winter over northern Europe with the strongest correlations for southern Finland and southwestern Norway (Uvo 2003; Zveryaev 2004). Wibig (1999) found that SCA correlates to unusually low precipitation over northern to northeastern Europe and unusually high precipitation in the Mediterranean and over Iceland. This is in agreement with the results of Jaagus (2009) who stated that positive (negative) phase of SCA gives decreased (increased) precipitation over the Scandes and Lapland. Additionally, Zveryaev (2004) found that the second leading mode of precipitation variability during winter in Europe resembles the EA. The EA was furthermore found to positively correlate with precipitation in northern and southern Europe and negatively over western Europe (Wibig 1999).

During summer the SNAO has been identified to affect precipitation over the British Isles, France, large parts of southern Europe and Scandinavia (Boé et al. 2009; Folland et al. 2009). Additionally, Zveryaev (2004) found that the northeastern part of Scandinavia receives increased precipitation when the SNAO is in a positive phase. AL has an impact on the precipitation over western Europe, causing dry conditions over western Europe and southern Scandinavia, while the AR affects northern and southern Europe causing wetter than normal circumstances (Boé et al. 2009).

In Europe, the precipitation is additionally considerably affected by the orography. A positive correlation has been noted between late winter precipitation and the NAO, which is especially notable over southern Norway and northern Sweden where a strong gradient lies. The occurrence of the strong precipitation gradients over these relatively small areas can be explained by the mountain ranges on the western side of the Scandinavian inland and the lee-effect they induce (Gouveia et al. 2008). Additionally, Uvo (2003) found that when focusing on Scandinavia, the leeward side of the Scandes show an opposite precipitation variability in contrast to the rest of the region. Thus, these mountains have an important role in preventing the moist winds induced by the positive NAO to reach the leeward side (Uvo 2003). Furthermore, both Jaagus (2009) and Uvo (2003) reach the conclusion that the precipitation on the leeward side of the Scandes is likely dependent on easterly winds carrying moisture from the Baltic Sea, and in contrast the precipitation over Norway and southern Finland is likely dependent on the positive NAO-induced westerly winds that bring moisture from the Atlantic. Hence, during winter, the source for precipitation along the Norwegian coast is the combined effect of the positive NAO-induced Atlantic winds and orographic lifting while precipitation in eastern Scandinavia and central Sweden is less influenced by the NAO because of the Scandes (Jaagus 2009; Uvo 2003).

3.3 Terrestrial carbon cycle and climate variability

Although it has high variability in between years, the terrestrial C-cycle in Europe is regarded as a net sink for carbon (Smith et al. 2020). Impacts on the C-cycle due to climate or weather extremes can, according to Frank et al. (2015), be divided into four categories consisting of the four possible combinations of two dimensions: direct and indirect, concurrent and lagged. The first two terms refer to how the impact emerges. Direct impacts are immediately caused by the extreme climatic event, but only if the limit for climatic stress is exceeded. On the contrary, an indirect impact would be when a climate extreme causes the ecosystem to become more susceptible to forcing. When the impact thereafter occurs, its forcing was not included in the climate extreme. The two remaining terms refer to when in time the impact occurs in relation to the climate extreme, where concurrent impacts appear concurrently to the climate extreme. A lagged impact is instead when the response of the ecosystem endures longer than the duration of the climate extreme, or when the response from the ecosystem appears some time after the climate extreme (Frank et al. 2015).

Photosynthetic activity and net carbon acquisition of vegetation vary diurnally, seasonally and annually during which the limiting resources also differs (Chapin et al. 2011). Through biogeochemical modelling of the importance of climatic controls for annual NPP

it has been shown, by Churkina & Running (1998), that in higher latitudes temperature has the largest influence. In middle latitudes, the combination of temperature and radiation or temperature and water availability was found to control the annual NPP. Water availability is the sole climatic control which limits annual NPP in lower latitudes (Churkina & Running 1998). A similar result was obtained by Nemani et al. (2003) who explored monthly climate statistics to calculate the contributions of the climate constraints radiation, temperature and precipitation of the global vegetation as NPP. The study concluded that water limitation mainly occurs in the subtropics, whereas temperature limitation is found in the northern regions and radiation limitation is observed in the tropics. Hence, vegetation growth is radiation limited in most of Europe except the northern parts where it is limited by both radiation and temperature (Nemani et al. 2003).

When averaged globally, von Buttlar et al. (2018) observed that GPP decreases noticeably during events of water limitation. Ecosystem respiration was also found to decrease during these events causing the effect on the net carbon balance to remain relatively unchanged. Larger effects were notable when extreme drought and heat events coincided which caused a strong decrease in both GPP and the net carbon balance. The concurrent events of drought and heat extremes was additionally shown by von Buttlar et al. (2018) to have the largest negative impact on the net carbon balance. Furthermore, it has been shown that the most significant impact on GPP is the duration of the extreme climatic event, where longer duration causes more severe effects. However, it is also important to note that there are some differences between different biomes. An example is boreal ecosystems, where a strong increase of GPP was observed during events of extreme heat in contrast to much smaller changes of GPP for other ecosystems (von Buttlar et al. 2018).

The responses of C-cycle and primary production have been studied during extreme events of drought and heat. An example is the European heat wave of 2003. During the summer of 2003, negative anomalies of primary production were detected (Reichstein et al. 2007). According to Reichstein et al. (2007), the anomaly was mainly the effect of water limitation. During summer 2018 another drought event hit Europe, which caused the vegetation productivity to decrease in northwestern Europe, including parts of Scandinavia. The decrease in productivity was found to be related to a lower precipitation and higher temperatures. Through modelling, it was determined that what affected the reduction of GPP most was low soil moisture (Smith et al. 2020).

3.3.1 Terrestrial carbon cycle and North Atlantic teleconnections

Since vegetation and the C-cycle are highly affected by climate variability and extreme climatic events, the conclusion can be drawn that the teleconnections should have an impact on the terrestrial C-cycle. When investigating the correlation between NDVI in spring and indices for nine teleconnection patterns on the Northern hemisphere (namely the Southern Oscillation, the NAO, the Arctic Oscillation, the Pacific-North American pattern, the Eurasian pattern, the West Pacific pattern, the West Atlantic pattern, the EA pattern and the North Pacific index), 71 % of the variability of GPP could be explained by them (Gong & Ho 2003).

Focusing especially on the North Atlantic and Europe, the wintertime NAO has a clear impact on vegetation greenness in spring as well as in summer. For northern Europe a

positive (negative) NAO index during winter has been found to promote high (low) NDVI in spring, but low (high) NDVI in summer. The induced response of the vegetation greenness is a lagged impact caused by the NAO due to its effect on winter temperature and precipitation, hence providing vegetation with warmer temperatures and better water availability (Gouveia et al. 2008). For vast areas in Scandinavia, Li et al. (2016) found similar results in form of a positive correlation between springtime vegetation and wintertime NAO, which was most pronounced in southern Scandinavia. Thus, Gouveia et al. (2008) and Li et al. (2016) found that the winter NAO can cause a lagged effect on springtime vegetation by affecting the temperature, creating more or less favourable conditions for spring phenology. On the other hand, the SCA in its positive phase wintertime brings large masses of cold air over major parts of Europe, including Scandinavia. This causes a decline in springtime NDVI which shows that the SCA, like the NAO, can have a lagged impact on springtime vegetation by affecting temperature (Gonsamo et al. 2016).

When considering the EA together with the NAO, the variability of the carbon sink in Europe can be even better understood. During negative phases of both EA and NAO, the net biome production increases the most, indicating a large uptake and thus an increased carbon sink. The meteorological variables causing this differ across the continent, since GPP is not showing a dependence of soil water in summer in Scandinavia in contrast to the rest of Europe. The anti-phases of EA and NAO cause different responses of the primary production. When EA has a negative phase and NAO a positive phase, a reduction in the carbon sink can be noted in all of Europe except for western Russia. This combination of phases produces a decreased biome production due to the combined decreases in both photosynthesis and respiration. The opposite combination of phases however is characterized by an increase of the carbon sink since photosynthesis increases in spring, but due to an additional increase of respiration during summer the increased carbon sink is not very strong (Bastos et al. 2016).

3.4 Empirical orthogonal functions (EOFs)

An EOF is a mathematical analysis concept which has been applied within atmospheric- and climate sciences since the 1940's. The practical aim of EOF analysis is, in the words of Hannachi et al. (2007), "finding a new set of variables that capture most of the observed variance from the data through linear combinations of the original variables". The application of EOF analysis on atmospheric and climate data has provided scientists with the ability to reduce the number of variables of an original data set, thus making it easier to handle while not losing nor affecting the variability of the data (Hannachi et al. 2007).

The EOF analysis fulfills the constraint of orthogonality in the spatial and temporal dimensions which has been identified as problematic for the physical interpretation of the results since physical modes rarely are orthogonal. Therefore, the technique of REOFs was developed. As the name indicates, it is a method where the EOFs are rotated with the purpose of easing the strict constraints of EOFs, mainly orthogonality. Additionally, the aim is to create more simple structures and making it possible to make physical interpretations of the obtained patterns (Hannachi 2004).

During the early years of the application to climate science, the EOF technique was used for prediction and smoothing purposes. During more recent years its application has been

extended to finding particular climate modes of variability (Hannachi et al. 2007). The teleconnections discussed in section 3.2 emerge as the leading EOFs of monthly SLP in the study by Fil & Dubus (2005) and of daily anomalies of SLP for Boé et al. (2007). Also, Moore et al. (2013) found the mentioned weather regimes as the leading EOFs of SLP in their study.

The following derivation of an EOF analysis is mainly based on Hannachi (2004) and G. Messori (personal communication, April, 2021). Climate data is often given as a three-dimensional data set that can be described as a field $F_{i,j,k}$ (Eq. 2). This field is a function of time t_i where $i = 1, ..., n$, latitude θ_j where $j = 1, .., p_1$ and longitude ϕ_k where $k = 1, .., p_2$.

$$F_{i,j,k} = F(t_i, \theta_j, \phi_k) \tag{2}$$

The data set to which an EOF analysis is to be applied consist of anomalies, i.e. data for which the climatology has been subtracted from each value. The field containing anomaly data is denoted $F'_{i,j,k}$. Given the three-dimensional anomaly field $F'_{i,j,k}$, the first step of an EOF analysis is to concatenate the two dimensions containing latitudes and longitudes, creating one single spatial dimension (Fig. 6).

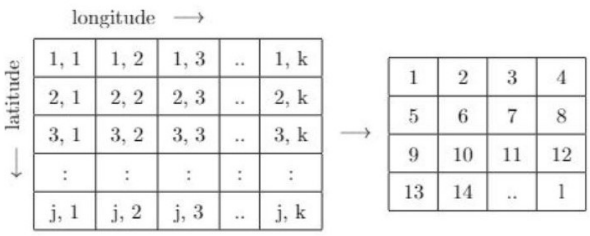

Figure 6: Schematic of the concatenation of the two spatial dimensions containing latitudes and longitudes (θ_j, ϕ_k) for a two-dimensional matrix.

The new spatial dimension is denoted s_l, where $l = 1, .., p_1 * p_2$. Consequently, the anomaly field $F'_{i,j,k}$ is decomposed into a field of two dimensions, a data matrix denoted $W'_{i,l}$ (Eq. 3).

$$F'_{i,j,k} \rightarrow W'_{i,l} = W'(t_i, s_l) \tag{3}$$

Next, the covariance matrix Σ of $W'_{i,l}$ is calculated (Eq. 4). The covariance matrix $\sum$ contains one value per pair of latitude-longitude grid points which gives a measure of how those grid points co-vary at every time step t_i.

$$\Sigma = \frac{1}{n} W'^{T}_{i,l} W'_{i,l} \tag{4}$$

As stated above, the purpose of performing EOF analysis is to identify linear combinations of all latitude-longitude grid points that explain the maximum variance of the original data set. Mathematically, this is equal to finding the direction vector $\bar{a}$ (Eq. 5). This vector has the property of maximizing the variance of the data set when it is multiplied with the matrix $W'_{i,l}$ (Eq. 6).

$$\bar{a} = (a_1, ..., a_p)^T \tag{5}$$

$$W'_{i,l}\bar{a} \rightarrow \text{maximum variability} \tag{6}$$

The maximum variance of the data set is found by first defining the variance of the multiplied matrices $W'_{i,l}\bar{a}$ (Eq. 7).

$$var(W'_{i,l}\bar{a}) = \frac{1}{n}\|W'_{i,l}\bar{a}\|^2 = \frac{1}{n}(W'_{i,l}\bar{a})^T(W'_{i,l}\bar{a}) = \bar{a}^T\Sigma\bar{a} \tag{7}$$

By requiring the direction vector $\bar{a}$ to be unitary, the final term of Eq. 7 maximized can be defined as Eq. 8.

$$\max_{\mathbf{a}}(\bar{a}^T\Sigma\bar{a}), \text{ s.t. } \bar{a}^T\bar{a} = 1 \tag{8}$$

The constrained maximum problem (Eq. 8) is solved as an eigenvalue problem (Eq. 9), where $\bar{a}$ contains the eigenvectors and λ the eigenvalues of the covariance matrix Σ.

$$\Sigma\bar{a} = \lambda\bar{a} \tag{9}$$

By solving the eigenvalue problem a number of p eigenvalues and eigenvectors are found, i.e. as many as the size of the spatial dimension. By arranging the found eigenvectors in decreasing order, the EOFs of the data set are the identified eigenvectors. In other words, the m:th eigenvector $\bar{a}_m$ of the covariance matrix Σ is the m:th EOF, where $m = 1, ..., p$. The explained variances are the identified eigenvalues extracted as the diagonal elements. In other words, the m:th eigenvalue λ_m provides a measure of how much of the variance is explained by the associated m:th EOF. The measure of explained variance can be rewritten as the percentage of variance explained (Eq. 10).

$$\text{percentage variance explained} = \frac{100 * \lambda_m}{\sum_{m=1}^{p}\lambda_m} \tag{10}$$

The full set of EOFs and eigenvalues together account for 100 % of the variance of the original data set. However, not every individual EOF and eigenvalue provide insight or are separate from the neighboring EOFs and eigenvalues. The number of EOFs to select for analysis can be determined by applying North's rule of thumb (North et al. 1982) which states: "...if the sampling error of a particular eigenvalue $\lambda[\delta \sim \lambda(2/n)^{1/2}]$ is comparable to or larger than the spacing between λ and a neighboring eigenvalue, then the sampling errors for the EOF associated with the λ are comparable to the size of the neighboring EOF", where n is the degrees of freedom of the data set. This essentially means that the eigenvalues which lie within the confidence interval of a neighboring eigenvalue cannot be differentiated from the neighbor (North et al. 1982).

By reshaping the eigenvectors $\bar{a}_m$ (Eq. 11), spatial patterns $A_m(\theta_j, \phi_k)$ are obtained. These spatial patterns show the variability patterns of each EOF.

$$\bar{a}_{m,l} \rightarrow A_m(\theta_j, \phi_k) \tag{11}$$

By then projecting the data set $W'_{i,l}$ onto the EOFs (Eq. 12), associated time series called principal components (PCs), c_m, are produced. To each EOF there is a corresponding PC.

$$c_m(t) = \sum_{s=1}^{p} W'(t,s)a_m(s) \tag{12}$$

At each time step, a PC can be interpreted as a measure of how similar the anomaly data is to the spatial pattern of the corresponding EOF.

4 Methods

All data processing performed in the present study was done via MATLAB, unless stated otherwise. Versions R2018b and R2021a of MATLAB were used. Additionally, the MATLAB toolbox NCTOOLBOX (Schlining et al. 2013) was utilized for aggregation of the NDVI data, described in section 4.2.1.

4.1 Precipitation

4.1.1 Data

The precipitation data analysed in the present study was obtained from the fifth generation of reanalysis data (ERA5) from the European Centre for Medium-Range Weather Forecasts (ECMWF). Reanalysis climate data is generated when global climate models are constrained with meteorological observations, thus producing numerical reconstructions of the climate and weather of the past. The reanalysis data includes estimated values of different atmospheric and surface parameters. ERA5 provides data from 1979 to today at an hourly temporal resolution and a 0.25° latitude x 0.25° longitude horizontal resolution (Hersbach et al. 2020). The precipitation data was downloaded within the geographical domain of Scandinavia, here bounded by latitudes 54.3° to 71.6° and longitudes 3.8° to 24.5° (Fig. 7) for each month between March to August for each year between 1981 to 2014. The time period was chosen to match the available NDVI data. Thereafter, the cumulative precipitation for each day at every latitude and longitude was summed. Based on these daily values, the cumulative precipitation for each month was summed. The monthly cumulative sums in March, April and May are from here on referred to as "monthly accumulated spring precipitation" and the monthly cumulative sums in June, July and August as "monthly accumulated summer precipitation".

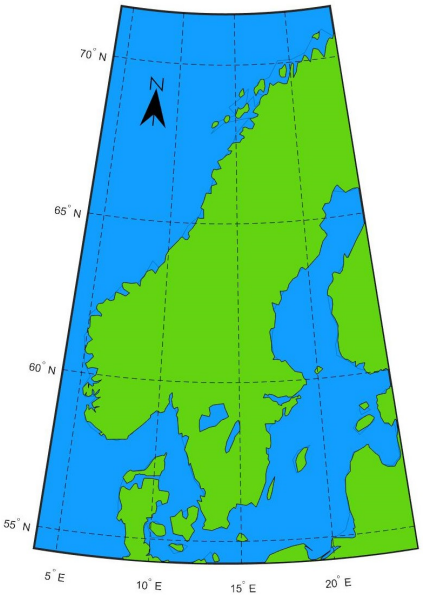

Figure 7: Geographical domain defined as Scandinavia, bounded by latitudes 54.3° to 71.6° and longitudes 3.8° to 24.5°.

The following method was applied to both the monthly accumulated spring precipitation and the monthly accumulated summer precipitation. For simplicity, the method below is however described using the general term "monthly accumulated precipitation" which thus includes the accumulated precipitation in both spring and summer. The gridded data of monthly accumulated precipitation has the structure of a three-dimensional field (Eq. 2). Because the spatial resolution of the data had a grid format of latitude x longitude and the Earth is spherical, 1° longitude becomes smaller with increasing lati-

tude. Consequently, the data points are more densely distributed when approaching the poles. To account for this, area weighting was performed on $F_{i,j,k}$ (Eq. 13) by weighting, for each latitude, all longitudes and time steps with the square root of cosine of the associated latitude (Hannachi 2004). This yielded the weighted field $\tilde{F}_{i,j,k}$, composed of the data set of monthly accumulated precipitation.

$$\tilde{F}_{i,j,k} = F_{i,j,k}\sqrt{cos(\theta_j)} \tag{13}$$

Next, the climatology of monthly accumulated precipitation was calculated for each month during the period 1981 to 2014 by calculating the average accumulated precipitation during the time period for each month. Then, anomalies of the monthly accumulated precipitation were calculated for each monthly value of the accumulated precipitation by removing the climatology of the month in question, thus producing a weighted anomaly field. The anomalies of the monthly accumulated precipitation are from here on named "monthly spring precipitation anomalies" and "monthly summer precipitation anomalies".

Finally, yearly precipitation anomalies were obtained for spring and summer separately. As the monthly spring precipitation anomalies were averaged, the average accumulated precipitation anomalies of March, April and May were produced for each year. These are henceforth referred to as "spring precipitation anomalies". The monthly summer precipitation anomalies were likewise averaged, producing the average accumulated precipitation anomalies of June, July and August for each year. From here on these are referred to as "summer precipitation anomalies".

Additionally, a Mann-Kendall trend test was applied to the mean yearly accumulated precipitation based on March, April and May and June, July and August separately using RStudio. The magnitude of the trends were decided by applying Sen's Slope which provided a measure of the increase or decrease in mm/spring month or mm/summer month.

4.1.2 EOF analysis

An EOF analysis was applied on the spring precipitation anomalies and the summer precipitation anomalies separately. Hence, the following procedure applies to both of the individual data sets. Initially, the two dimensions containing latitudes and longitudes were concatenated, creating one single spatial dimension of combined latitudes and longitudes (Eq. 3). Next, the covariance matrix of the concatenated anomaly data set was defined (Eq. 4). From the covariance matrix, the EOFs and the eigenvalues were obtained.

Following, the number of EOFs to keep and analyse was determined by applying North's rule of thumb (North et al. 1982). As many EOFs as the size of the spatial dimension were obtained, but the EOFs that explain most of the variability and are separate from their neighbors are among the first few EOFs. Therefore, the first ten eigenvalues were plotted with their sampling errors (Fig. 9, Fig. 15). By analysing the first ten EOFs the limit where the EOFs became indistinct from their neighbors was assumed to be included. However, the degrees of freedom used was the number of grid points; an overestimation that made the choice of distinct EOFs overly stringent. Because of thus,

a strict application of North's rule of thumb would have excluded all EOFs. However, since the degrees of freedom were overestimated, a somewhat more loose interpretation of the rule was applied. Such an interpretation meant the overlap between the sampling error and the percentage of variance explained was considered, as opposed to an overlap between sampling errors.

The concatenated precipitation anomalies were then projected onto the selected EOFs, producing the corresponding PCs. The PCs were standardized by dividing each of the PCs by the standard deviation of the PC in question.

4.2 NDVI

4.2.1 Data

The NDVI data analysed in the present study, originally from satellite data by NASA, came from the recently published study by Wu et al. (2021). The data had a biweekly temporal resolution and a 0.5° latitude x 0.5° longitude spatial resolution. Initially, the grid points constrained by the latitudes 54.3° to 71.6° and longitudes 3.8° to 24.5° (Fig. 7) were extracted for all 12 months between 1981 to 2014. All NDVI values equal to or lower than 0.1 were removed, i.e. set as "NaN", to exclude non-vegetation surfaces such as bare soil, rocks and snow. Thereafter, monthly averages were calculated. The value for each time point was the maximum composite during a biweekly retrieval period. Hence, the average for a month was calculated based on the values for the 16th of the month in question and the 1st of the successive month. During leap years, the data was available for the 1st, 16th and 29th of February, causing the other months to have data points either the 15th and 30th or the 15th and 31st. Therefore, during leap years, the average for January was based on the 16th of January and the 1st of February, the average for February was based on the 16th and 29th of February, the average for March was based on the 15th and 30th of March and so on.

Seasonal trends of increasing NDVI in the Northern Hemisphere have been observed (e.g. Eastman et al. 2013; Zhou et al. 2001) and due to this the data was detrended by calculating the average NDVI each year and then, for every month, subtracting the yearly average associated to that month. Next, data in June, July and August was extracted from each year and the average NDVI each year during these months was calculated. Then, the climatology of the monthly detrended NDVI was calculated for each month during the time period by calculating the average detrended NDVI during the time period for each month. From each detrended monthly average, the climatology of the month in question was removed, thus producing detrended monthly average NDVI anomalies. From these values June, July and August were extracted from each year. These detrended monthly average NDVI anomalies in June, July and August respectively are henceforth called "monthly NDVI anomalies". Lastly, detrended yearly average NDVI anomalies were obtained through the averaging of the detrended monthly average NDVI anomalies in June, July and August each year. These values are hereafter referred to as "NDVI anomalies".

Because of the effect of lagged soil memory, the data set of monthly NDVI anomalies had a risk of confounding and mixing the signals from the vegetation and the climate (M. Wu, personal communication, April, 2021). By instead calculating yearly NDVI anomalies,

the interannual variability was extracted as the seasonal signals were excluded. However, much fewer data points were available compared to the monthly NDVI anomalies. By calculating both monthly and yearly NDVI anomalies, the results of the yearly NDVI anomalies could be evaluated in relation to the results of the monthly NDVI anomalies so any large differences which might be due to the size of the data set were possible to detect.

4.2.2 NDVI analysis

The following analysis was separately applied to the results from the EOF analysis of spring precipitation anomalies and summer precipitation anomalies. Anomalous events in the PCs of precipitation anomalies were identified for which the relationship between the precipitation anomalies and the NDVI anomalies was to be analysed. From each PC a total of ten years were chosen, equivalent to the five largest and the five lowest values, hence the ten years with the most anomalous precipitation events were analysed (Fig. 11, Fig. 17). The choice to investigate five anomaly years of each sign was arbitrary as the conditions for the selected number was that too few years would not yield any significant results, while too many years would not represent anomalous events. The mean NDVI anomalies during the positive anomaly years was calculated for each PC, as well as for the negative anomaly years. Additionally the difference of the mean NDVI anomalies between the positive and the negative PC anomaly years was calculated for each PC. Thus, three two-dimensional matrices of mean NDVI anomalies were created for each PC.

The statistical significance of the mean NDVI anomalies was evaluated through Monte Carlo simulations. Two sets of five years between 1981 to 2014 were randomly chosen, the same number of years as was chosen from the PCs in total. For each of the two sets, the average of the NDVI anomalies was calculated, and after calculating the difference between the two sets, the mean of this difference was additionally calculated. The procedure was repeated 1000 times and afterwards the one-tailed 10 % significance test was performed. This significance level was chosen to ensure signals would emerge while still being strict enough to draw conclusions from. For the five positive and the five negative years originally identified in the PCs, the mean NDVI anomalies that were lower (higher) than the 10th (90th) percentile of the simulated values were identified. The significant values of mean NDVI anomalies of the difference between the five positive and the five negative PC anomaly years were also identified by finding the values lower (higher) than the 10th (90th) percentile of the simulated difference between the two sets of NDVI anomalies.

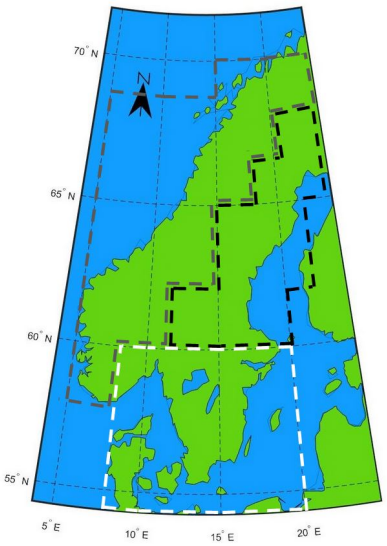

Figure 8: Geographical domain of the present study divided into three regions. The white square is named "southern Scandinavia", the black shape "central- and north-eastern Sweden" and the dark grey shape "Norway".

Regional means were additionally calculated for the difference in mean NDVI anomalies between positive and negative PC anomaly years. Scandinavia was divided into regions based on the updated climate classifications originally constructed by Köppen and Geiger (Kottek et al. 2006). This resulted in three regions representing roughly three different climate classifications - southern Scandinavia (region one), central- and northeastern Sweden (region two) and Norway (region three) (Fig. 8). As different plant species can cause variations in NDVI, comparisons between different ecosystems should be done cautiously (Chapin et al. 2011). By calculating regional averages for regions based on climate classifications this potential issue was minimized. To account for the spherical shape of the Earth, the difference in mean NDVI anomalies between positive and negative PC anomaly years were, at each latitude, area-weighted by the cosine of the latitude in question, i.e. at each latitude θ_j multiplied with $cos(\theta_j)$. The difference of mean NDVI anomalies were additionally normalized by the average cosine of the latitude. Then, averages were calculated for each region. The statistical significance of the regional means was evaluated through Monte Carlo simulations. Following the same Monte Carlo simulation procedure as described above, regional means were calculated 1000 times followed by the performance of a one sided 10 % significance test.

4.3 Teleconnection patterns

4.3.1 Indices

Numerical values of teleconnection indices were obtained from the National Weather Service Climate Prediction Center (NOAA National Weather Service Climate Prediction Center 2012). The indices had a monthly temporal resolution and had been calculated through the application of REOFs (NOAA National Weather Service Climate Prediction Center 2012). Initially, data was extracted for the time period 1981 to 2014. Then, the data of June, July and August was extracted from the time period. Next, the indices were converted from monthly values to yearly averages based solely on the values during June, July and August. The teleconnections NAO, EA and SCA were selected and analysed due to their relevance and availability. Since the indices were only investigated during summer, the NAO index used is henceforth called the "SNAO index".

4.3.2 Teleconnection analysis

The analysis of the relation between the precipitation anomalies and North Atlantic teleconnections was solely performed for the summer precipitation anomalies. Initially, time series of the teleconnection indices were created for the SNAO, EA and SCA separately. Additionally, for each time series, the five years of positive anomalies and the five years of negative anomalies identified from each PC were marked. The relation between the obtained PCs and the teleconnection index time series was analysed and for each combination of an individual PC and an individual teleconnection index, the Pearson correlation coefficient R was calculated as well as the p-value evaluating the significance of R. Thus, the precipitation and NDVI data were assumed to be normally distributed. R was deemed statistically significant if $p < 0.05$ since it was the default significance level.

5 Results

The results from the analyses based on monthly spring precipitation anomalies, monthly summer precipitation anomalies and monthly NDVI anomalies are presented in Appendix A.3 to A.10.

5.1 Spring precipitation

5.1.1 EOF analysis

Based on the first ten eigenvalues and their sampling errors, the number of EOFs selected for analysis of the spring precipitation anomalies was determined (Fig. 9). The upper limit of the sampling error of the second eigenvalue is below the percent of variance explained by the first eigenvalue. Therefore, these eigenvalues and thus their corresponding EOFs are assumed to be separate. However, the upper limit of the sampling error of the third eigenvalue is very close to the percent of variance explained by the second eigenvalue. Additionally, the upper limit of the sampling error of the fourth eigenvalue is clearly larger than the percent of variance explained by the third eigenvalue. There is thus a possibility that the third eigenvalue is mixed with either the second or fourth eigenvalue. Therefore, the third eigenvalue is provisionally included in the analysis while being aware of it likely being degenerate. The remaining eigenvalues, following the third eigenvalue, are excluded since they are not deemed to be separate.

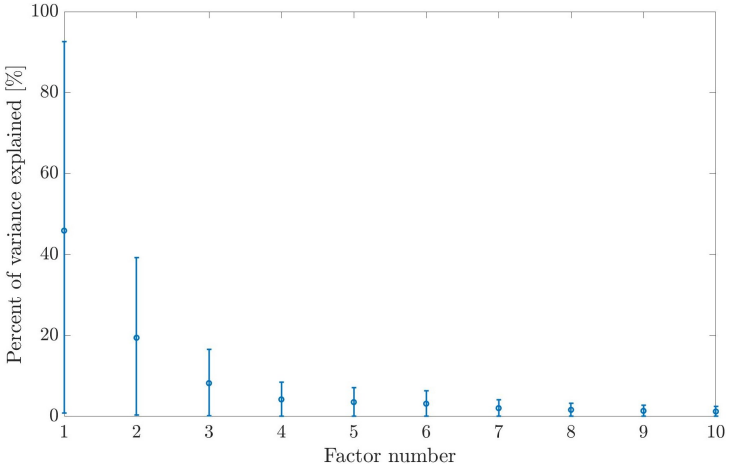

Figure 9: The percent of variance explained by the first ten eigenvalues of mean yearly spring precipitation anomalies, with the associated sampling errors.

The patterns given by the first three EOFs, based on spring precipitation anomalies, explains 45.9 %, 19.4 % and 8.20 % respectively of the variance (Fig. 10). EOF1 has coherent precipitation variability along the entire Norwegian coast, with strong anomaly centers in the middle and the southern parts. The rest of the Scandinavian inland has very weak weight for EOF1. EOF2 has opposite precipitation variability between the upper Norwegian coast and the rest of the Scandinavian inland, while EOF3 has opposite precipitation variability between the southern tip of Norway and the rest of Scandinavia.

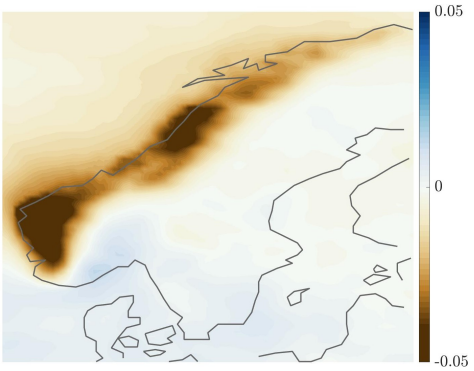

(a) EOF1 (explains 45.9 %).

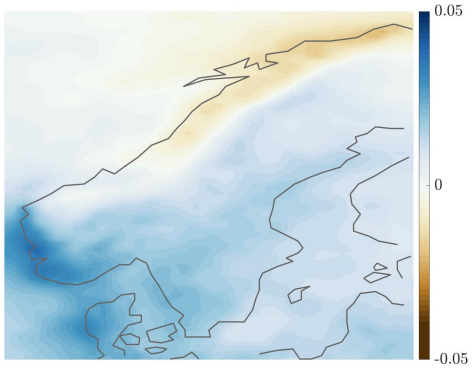

(b) EOF2 (explains 19.4 %).

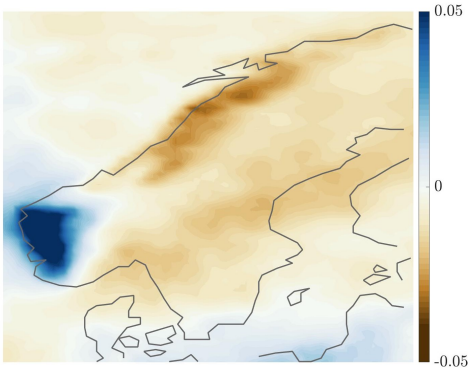

(c) EOF3 (explains 8.20 %).

Figure 10: Spatial patterns of the first three empirical orthogonal functions (EOFs) chosen for analysis. The spatial patterns show the variability of mean yearly spring precipitation anomalies, based on cumulative precipitation in March, April and May in Scandinavia 1981 to 2014. The colorbar shows the precipitation anomalies in mm/spring month.

For each of the EOFs, there is an associated time series. In these PCs, the five most positive and the five most negative years are marked, i.e. the years where the corresponding spatial pattern is most alike the spring precipitation anomalies (Fig. 11).

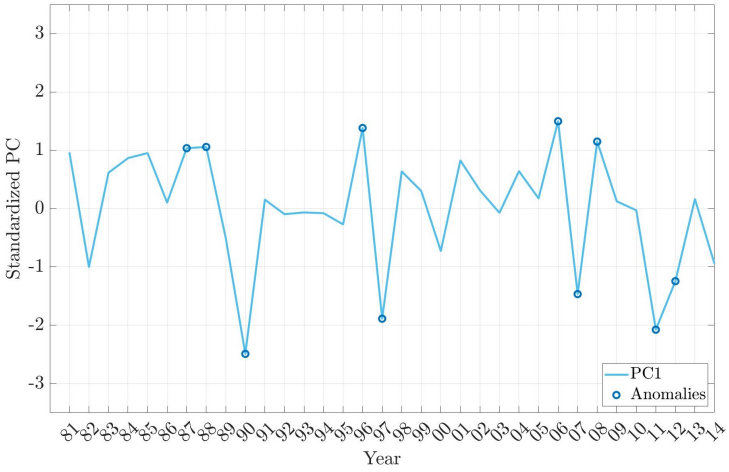

(a) Standardized PC1.

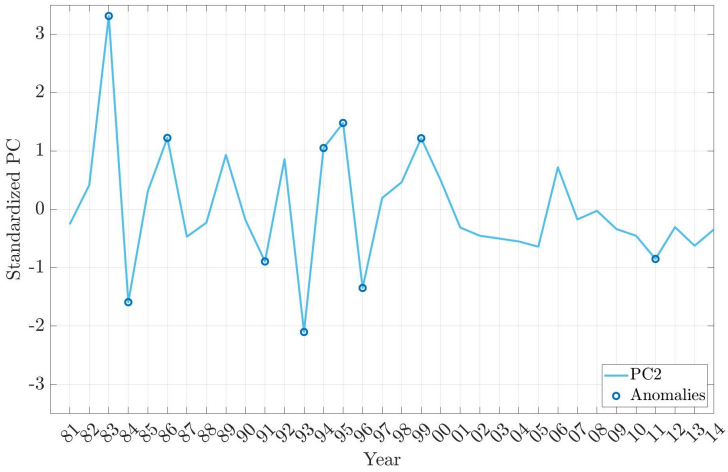

(b) Standardized PC2.

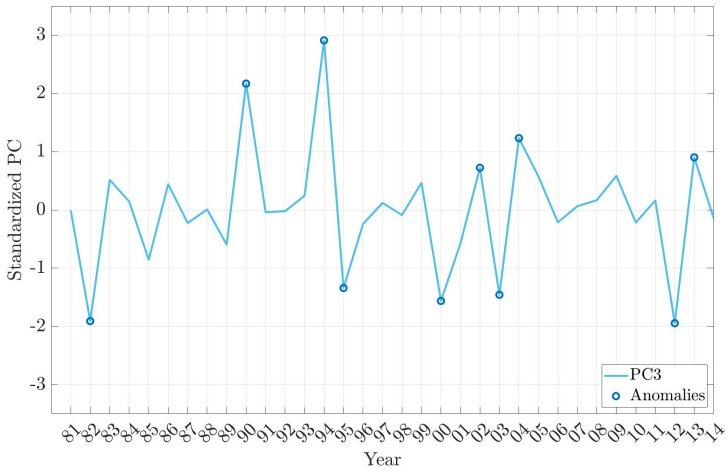

(c) Standardized PC3.

Figure 11: Standardized principal components (PCs) corresponding to the first three empirical orthogonal functions (EOFs) of mean yearly spring precipitation anomalies. The mean anomalies are based on cumulative precipitation in March, April and May in Scandinavia 1981 to 2014. For each PC the five largest and the five lowest values are marked, showing years of anomalous precipitation variability.

The precipitation during March, April and May did not reveal any statistically significant trends in any land area (Fig. 12).

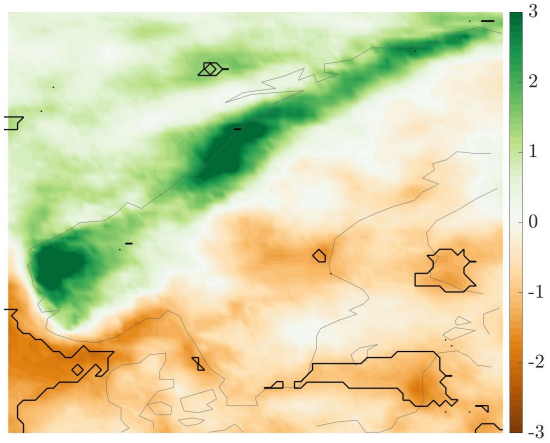

Figure 12: Trends of yearly mean accumulated precipitation during March, April and May (spring). Statistically significant trends at the 95 % level are encircled by black lines.

5.1.2 NDVI analysis

Per PC, the mean NDVI anomalies during years of positive PC anomalies, of negative PC anomalies and of the difference between positive and negative PC anomaly years are presented. An attempt at analysing the mean NDVI anomalies corresponding to PC3 was made, but since these figures did not provide any coherent regions of statistically significant anomalies, they are not discussed further. The resulting figures from PC3 are shown in Appendix A.1.

During both the positive and the negative anomaly years of PC1, few statistically significant areas of mean NDVI anomalies are found (Fig. 13). There are mainly two large statistically significant areas during the positive anomaly years, occurring in eastern Sweden and northern Scandinavia. The negative anomaly years shows some statistically significant areas in the central inland and northeastern Swedish coast. These areas mainly coincide with negative mean NDVI anomalies. The areas of statistical significance are also few for the difference in mean NDVI anomalies between positive and negative PC1 anomaly years (Fig. 13). Some are found in the central inland, while some occur in the middle of the Norwegian coast, but there is not an apparent pattern noticeable among these.

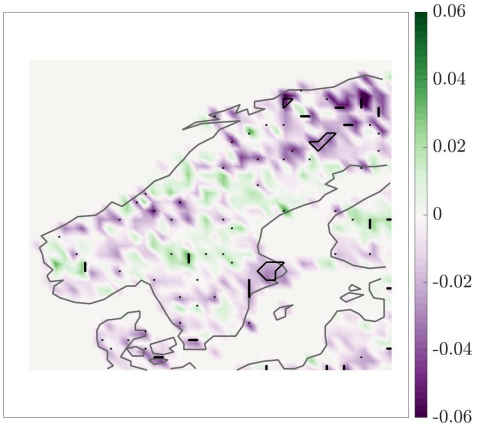

(a) Mean yearly summer NDVI anomalies during positive PC1 anomaly years.

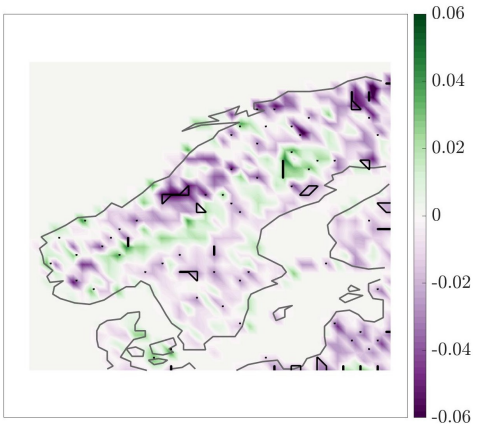

(b) Mean yearly summer NDVI anomalies during negative PC1 anomaly years.

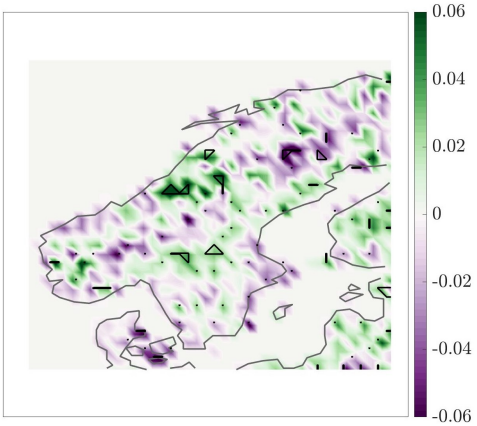

(c) The difference in mean yearly summer NDVI anomalies between positive and negative PC1 anomaly years.

Figure 13: Mean yearly summer NDVI anomalies during anomaly years of the first principal component (PC1) of yearly accumulated precipitation anomalies in March, April and May in Scandinavia 1981 to 2014. Statistically significant anomalies at the 90 % level are encircled by black lines. The NDVI anomalies are based on yearly averages of NDVI in June, July and August in Scandinavia 1981 to 2014.

The statistically significant areas of the positive anomaly years of PC2 seem to predominantly include positive mean NDVI anomalies and mainly occur in southern Scandinavia (Fig. 14). For the negative anomaly years of PC2 the statistically significant areas have a clear pattern since the majority lie on a band following the mountainous regions (Fig. 14). These are of negative mean NDVI anomalies although there are a few statistically significant areas in southern Scandinavia coinciding with positive mean NDVI anomalies. For the difference in mean NDVI anomalies between positive and negative PC2 anomaly years, the areas of statistical significance have a similar pattern as for the negative anomaly years - on a band along the mountainous areas (Fig. 14). These are mainly positive mean NDVI anomalies. When comparing these results to the spatial pattern of EOF2, the line of significant areas for the difference in mean NDVI anomalies lies on the negative precipitation anomalies, almost on the border between the different signs (Fig. 10). This is also true for the statistically significant areas of negative mean NDVI anoma-

lies occurring during negative PC2 anomaly years. The statistically significant areas of positive mean NDVI anomalies of positive PC2 anomaly years corresponds to positive precipitation anomalies in southern Scandinavia (Fig. 10).

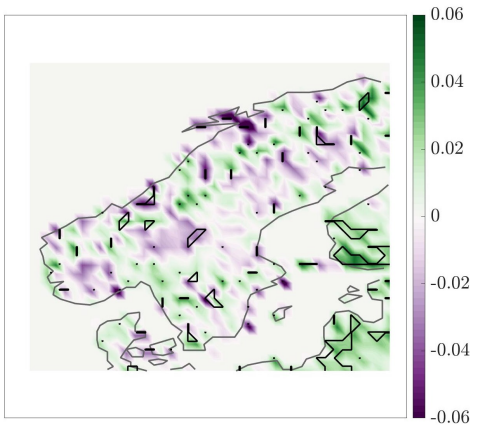

(a) Mean yearly summer NDVI anomalies during positive PC2 anomaly years.

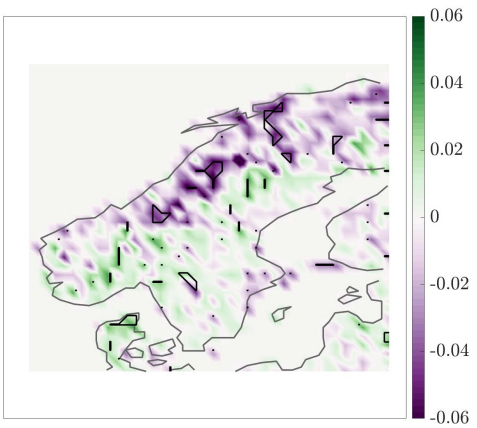

(b) Mean yearly summer NDVI anomalies during negative PC2 anomaly years.

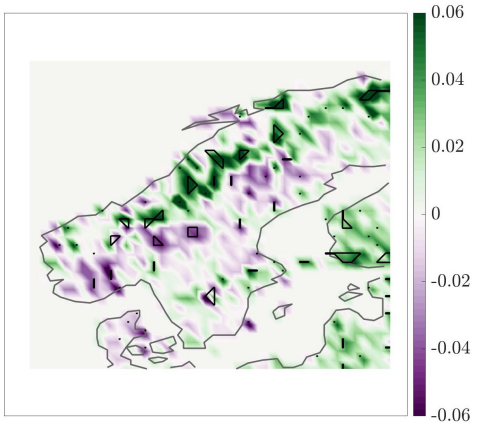

(c) The difference in mean yearly summer NDVI anomalies between positive and negative PC2 anomaly years.

Figure 14: Mean yearly summer NDVI anomalies during anomaly years of the second principal component (PC2) of monthly accumulated precipitation anomalies in March, April and May in Scandinavia 1981 to 2014. Statistically significant anomalies at the 90 % level are encircled by black lines. The NDVI anomalies are based on yearly averages of NDVI in June, July and August in Scandinavia 1981 to 2014.

Two of three regional averages of the difference in mean NDVI anomalies between positive and negative anomaly years of PC1 are negative, however none of the three are statistically significant (Table 1). The same is true for PC2 for which two of three regional averages of the difference in mean NDVI anomalies between positive and negative anomaly years are negative and neither one of the regional averages are statistically significant (Table 1).

Table 1: Regional average of the difference in mean yearly summer NDVI anomalies between positive and negative anomaly years for each principal component (PC). None of the anomalies are statistically significant at the 90 % level.

	Mean yearly summer NDVI anomaly	
	PC1	PC2
Southern Scandinavia	-0.0075	-0.00068
Central- and northeastern Sweden	-0.0022	-0.00035
Norway	0.0021	0.015

5.2 Summer precipitation

5.2.1 EOF analysis

The number of EOFs selected for analysis of the summer precipitation anomalies are decided by observing the first ten eigenvalues and their sampling errors (Fig. 15). The eigenvalues have the same configuration as the ones based on the spring precipitation anomalies, so the same motivation applies and the first three eigenvalues are included in the analysis while being aware that the third eigenvalue likely is degenerate. The remaining eigenvalues, following the third eigenvalue, are excluded since they are not deemed to be separate.

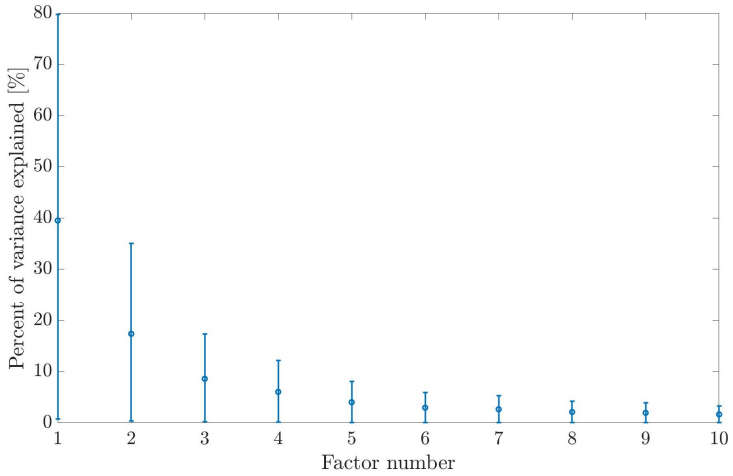

Figure 15: The percent of variance explained by the first ten eigenvalues of mean yearly summer precipitation anomalies, with the associated sampling errors.

The patterns given by the first three EOFs, based on summer precipitation anomalies, explains 39.5 %, 17.4 % and 8.59 % respectively of the variance (Fig. 16). EOF1 has an opposite precipitation variability along the upper Norwegian coast and the rest of the Scandinavian inland. The second EOF has a large area of coherent precipitation variability along the entire Norwegian coast and northern Scandinavia, and weak EOF weight in southern Scandinavia. EOF3 has an opposite precipitation variability in central and eastern Scandinavia and southern and northern Scandinavia.

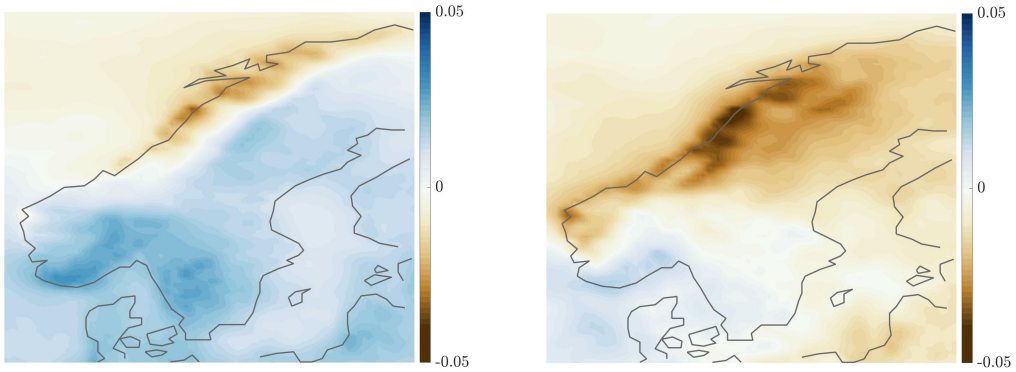

(a) EOF1 (explains 39.5 %). **(b)** EOF2 (explains 17.4 %).

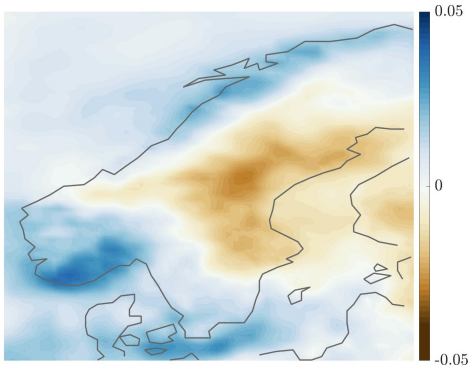

(c) EOF3 (explains 8.59 %).

Figure 16: Spatial patterns of the first three empirical orthogonal functions (EOFs) chosen for analysis. The spatial patterns show the variability of mean yearly summer precipitation anomalies, based on cumulative precipitation in June, July and August in Scandinavia 1981 to 2014.

For each of the EOFs, there is an associated time series. In these PCs, the five most positive and the five most negative years are marked, i.e. the years where the corresponding spatial pattern is most alike the spring precipitation anomalies (Fig. 17).

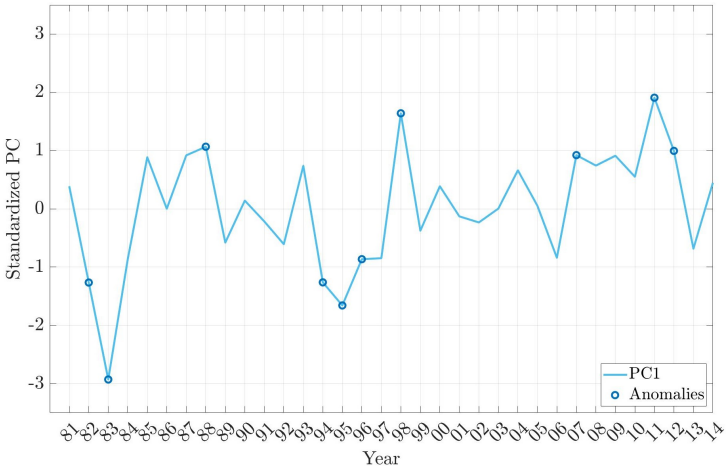

(a) Standardized PC1.

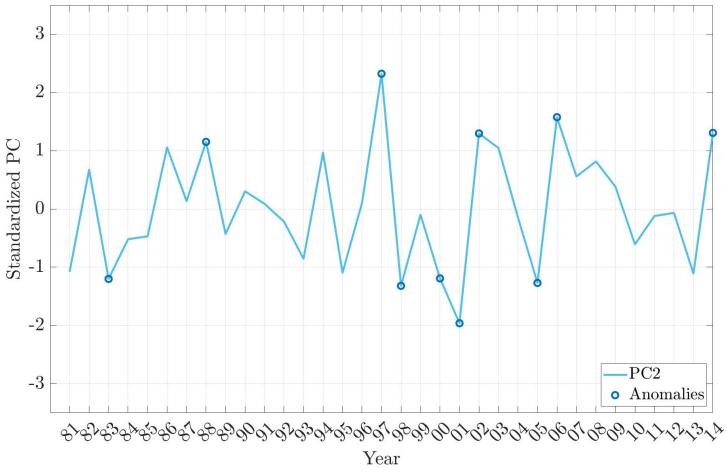

(b) Standardized PC2.

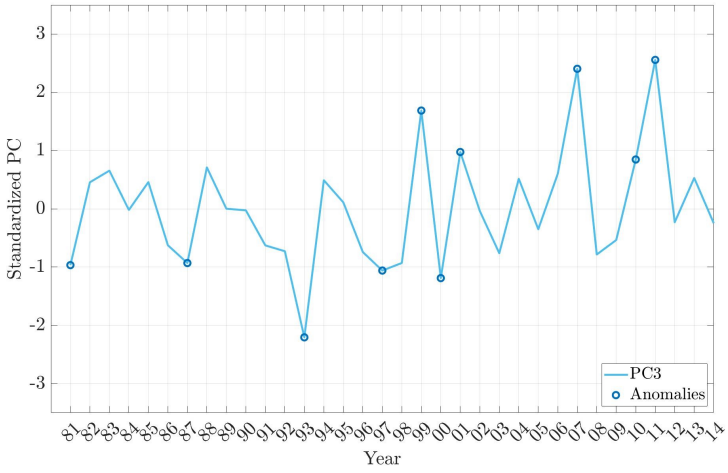

(c) Standardized PC3.

Figure 17: Standardized principal components (PCs) corresponding to the first three empirical orthogonal functions (EOFs) of mean yearly summer precipitation anomalies. The mean anomalies are based on the cumulative precipitation in June, July and August in Scandinavia 1981 to 2014. For each PC the five largest and the five lowest values are marked, showing years of anomalous precipitation variability.

The precipitation during June, July and August have statistically significant, positive trends in southern Scandinavia with a magnitude of three to four mm/summer month (Fig. 18).

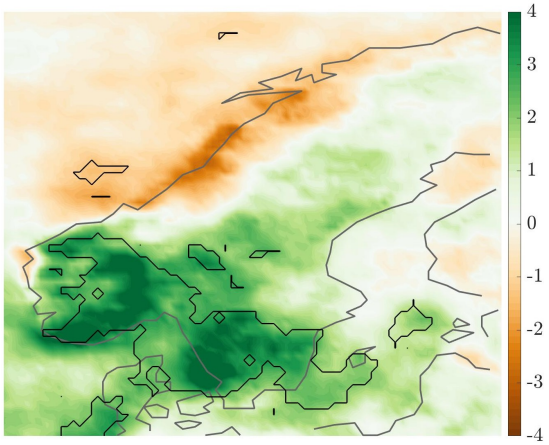

Figure 18: Trends of yearly mean accumulated precipitation during June, July and August (summer). Statistically significant trends at the 95 % level are encircled by black lines.

5.2.2 NDVI analysis

Per PC, the mean NDVI anomalies corresponding to the years of positive PC anomalies, of negative PC anomalies and of the difference between positive and negative PC anomaly years are presented. An attempt at analysing the mean NDVI anomalies corresponding to the anomaly years of PC3 was made; however they did not provide any coherent regions of statistically significant anomalies or meaningful information. Due to this, the results of PC3 were not analysed further and the resulting figures from PC3 are to be found in Appendix A.2.

The statistically significant areas of the mean NDVI anomalies are few during the positive anomaly years of PC1 (Fig. 19). However, the statistically significant areas corresponding to the negative anomaly years of PC1 have a more extensive coverage, which is also true for the difference between these from which a clearer signal emerges (Fig. 19). For the negative PC1 anomalies, the statistically significant mean NDVI anomalies are predominantly negative and mainly occur in central and northeastern Scandinavia. By comparison to the spatial pattern of EOF1 (Fig. 16), the three large southernmost statistically significant areas of negative PC1 anomaly years coincide with the positive summer precipitation anomalies which cover the entire Scandinavian inland. A cluster of large statistically significant areas are found in northeastern Scandinavia for the negative PC1 anomaly years, coinciding with weak positive summer precipitation anomalies. Regarding the difference between the positive and negative PC1 anomaly years, most of the statistically significant areas are of positive mean NDVI anomalies and lie along the Swedish east coast, thus coinciding with positive precipitation anomalies in EOF1.

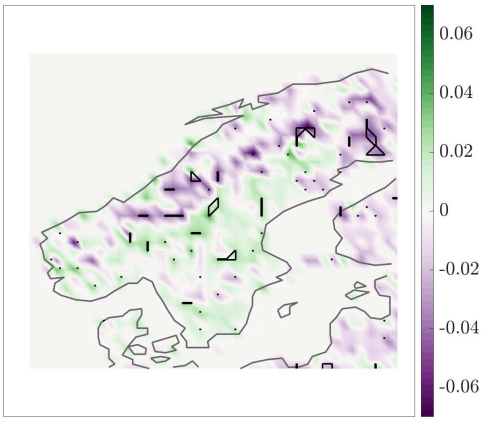

(a) Mean yearly summer NDVI anomalies during positive PC1 anomaly years.

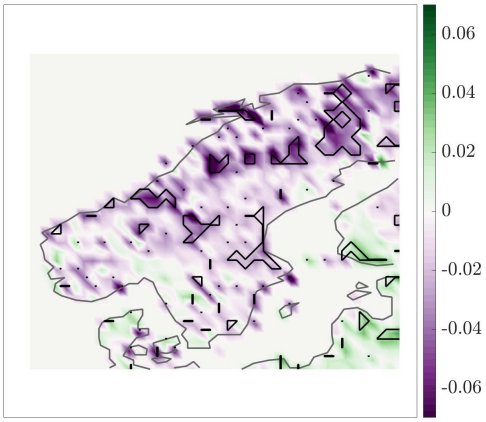

(b) Mean yearly summer NDVI anomalies during negative PC1 anomaly years.

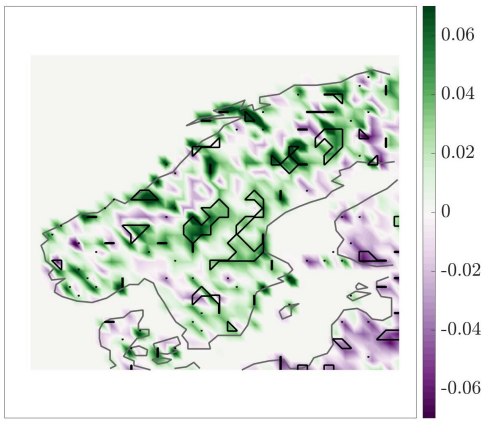

(c) The difference in mean yearly summer NDVI anomalies between positive and negative PC1 anomaly years.

Figure 19: Mean yearly summer NDVI anomalies during anomaly years of the first principal component (PC1) of monthly accumulated precipitation anomalies in June, July and August in Scandinavia 1981 to 2014. Statistically significant anomalies at the 90 % level are encircled by black lines. The NDVI anomalies are based on yearly averages of NDVI in June, July and August in Scandinavia 1981 to 2014.

Through observation of the mean NDVI anomalies of PC2 anomaly years, it is evident that there are several areas of statistical significance for both the negative PC2 anomalies and for the difference between the positive and negative PC2 anomalies (Fig. 20). The positive PC2 anomalies mainly correspond to positive statistically significant mean NDVI anomalies and these are scattered on the Norwegian coast (Fig. 20). The negative PC2 anomalies primarily give negative statistically significant mean NDVI anomalies in central Scandinavia. For the difference, the significant areas occur similarly to the areas given by the negative PC2 anomalies, which is the central Scandinavian inland. These statistically significant areas occur at positive mean NDVI anomalies. The few statistically significant areas of positive mean NDVI anomalies during positive PC2 anomaly years coincide with the area of large negative summer precipitation anomalies in EOF2 (Fig. 16). When comparing the statistically significant mean NDVI anomalies for the negative PC2 anomaly years and the difference between the positive and negative PC2 anomalies with EOF2, they coincide with both the areas of positive and negative summer precipitation

anomalies. The statistically significant areas in southern Norway and Sweden lie where EOF2 has weak positive summer precipitation anomalies, while the statistically significant areas in the central inland occur at negative summer precipitation anomalies in EOF2.

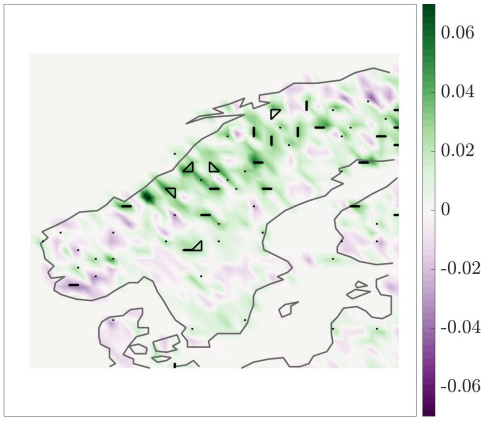

(a) Mean yearly summer NDVI anomalies during positive PC2 anomaly years.

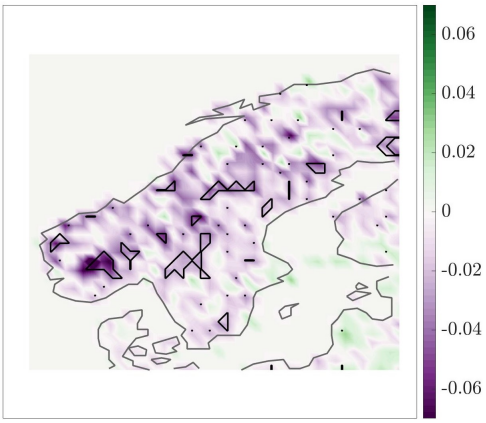

(b) Mean yearly summer NDVI anomalies during negative PC2 anomaly years.

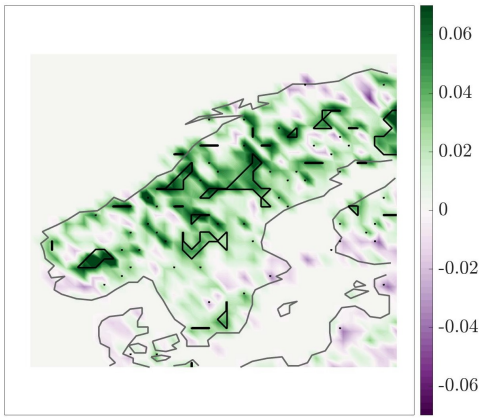

(c) The difference in mean yearly summer NDVI anomalies between positive and negative PC2 anomaly years.

Figure 20: Mean yearly summer NDVI anomalies during anomaly years of the second principal component (PC2) of monthly accumulated precipitation anomalies in June, July and August in Scandinavia 1981 to 2014. Statistically significant anomalies at the 90 % level are encircled by black lines. The NDVI anomalies are based on yearly averages of NDVI in June, July and August in Scandinavia 1981 to 2014.

The difference in mean NDVI anomalies between positive and negative PC anomaly years produced solely positive regional averages for the anomaly years of both PC1 and PC2 (Table 2). Additionally, during anomaly years of PC1 and PC2 the regional averages in central- and northeastern Sweden as well as in Norway are significant.

Table 2: Regional average of the difference in mean yearly summer NDVI anomalies between positive and negative anomaly years for each principal component (PC). Statistically significant values are marked with * at the 90 % level.

	Mean yearly summer NDVI anomaly	
	PC1	PC2
Southern Scandinavia	0.0091	0.0068
Central- and northeastern Sweden	0.017*	0.022*
Norway	0.019*	0.023*

5.2.3 Teleconnection analysis

The averages of the SNAO index during positive and negative PC1 anomaly years lie symmetrically on both sides of the zero line (Fig. 21) and a relation between the SNAO index and PC1 is confirmed by the Pearson test (Table 3). The SNAO index and PC1 have a strong negative relation which is the strongest among the combinations of teleconnection indices and PCs. However, there is not a relation between the SNAO and PC2.

During the anomaly years of PC1, the average EA index is placed symmetrically around zero for the positive and the negative anomaly years (Fig. 21). According to the correlation test there is also a statistically significant relation between PC1 and the EA index (Table 3). However, R is lower than R for the relation between PC1 and SNAO which indicates that the relation between PC1 and EA is not as strong. The average values of the EA index are just above zero for both the positive and negative years of PC2, but there is not a significant relation between the EA index and PC2 (Fig. 21, Table 3). The average SCA index, for both positive and negative anomaly years of PC1, is very close to zero (Fig. 21), and there is no statistically significant correlation between these two variables (Table 3). However, according to the correlation test, there is a statistically significant relation between PC2 and the SCA index with R of the same size as for PC1 and EA (Table 3).

Table 3: The correlation between the yearly average index, solely based on June, July and August, of the Summer North Atlantic Oscillation (SNAO), the East Atlantic pattern (EA) and the Scandinavian pattern (SCA) 1981 to 2014 and each principal component (PC). Statistically significant values at the 95 % level are marked with *.

	Teleconnection index	R
PC1	SNAO	-0.78*
	EA	0.44*
	SCA	-0.22
PC2	SNAO	-0.021
	EA	0.13
	SCA	0.45*

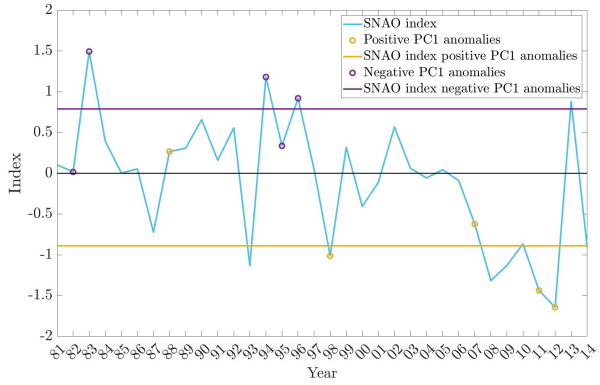

(a) SNAO index with PC1 anomaly years marked.

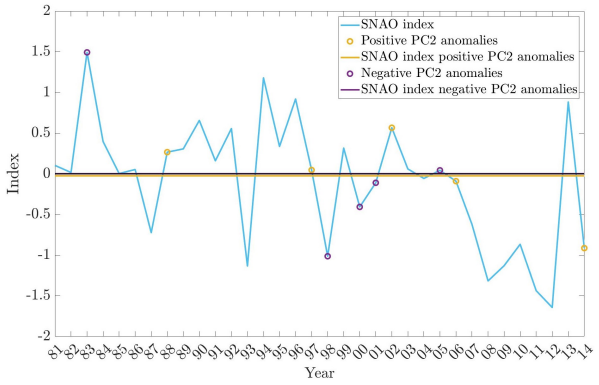

(b) SNAO index with PC2 anomaly years marked.

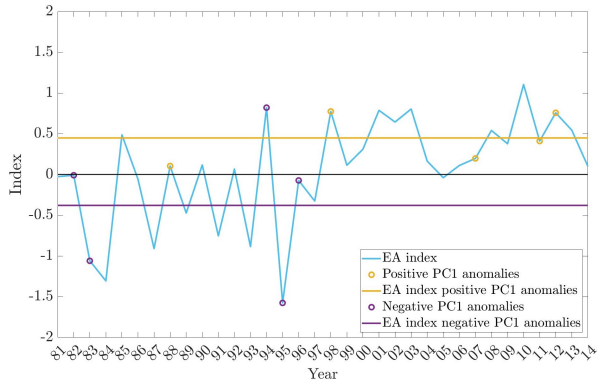

(c) EA index with PC1 anomaly years marked.

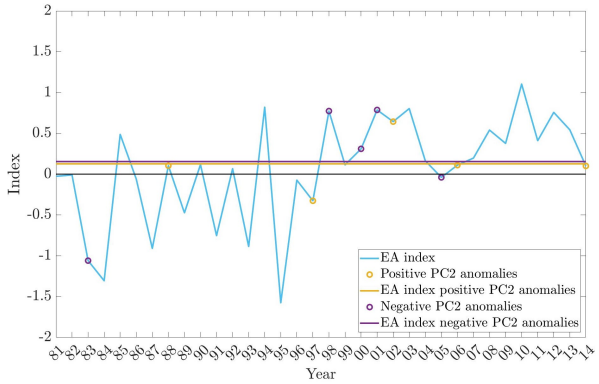

(d) EA index with PC2 anomaly years marked.

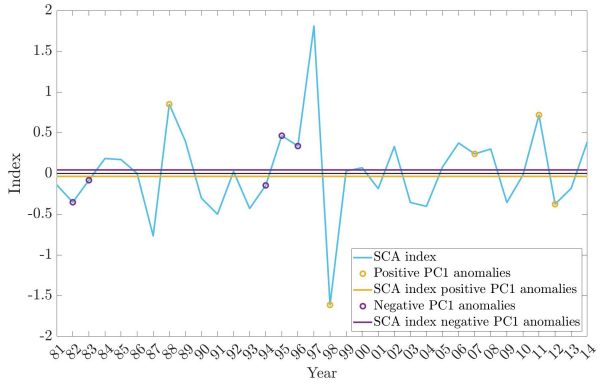

(e) SCA index with PC1 anomaly years marked.

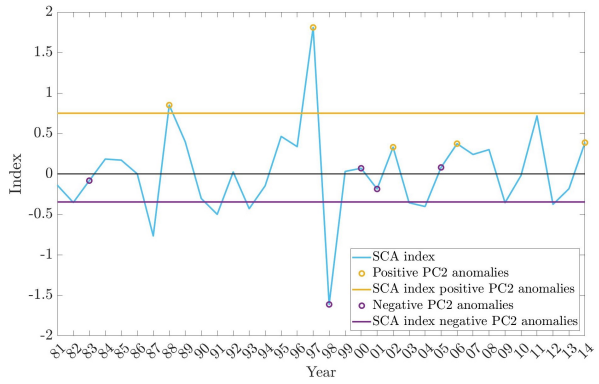

(f) SCA index with PC2 anomaly years marked.

Figure 21: The yearly average index, solely based on June, July and August, of the Summer North Atlantic Oscillation (SNAO), the East Atlantic pattern (EA) and the Scandinavian pattern (SCA) 1981 to 2014. The positive and the negative anomaly years of the first principal component (PC1) (left column) and of the second principal component (PC2) (right column) are marked. Additionally, the average value of the index during the positive and the negative years respectively is marked, to indicate if there is a tendency to a certain configuration of the teleconnection patterns during the years of anomalous precipitation.

6 Discussion

6.1 Data

The precipitation data and the NDVI data analysed in the present study are of different spatial resolutions, where the resolution of the precipitation is four times higher than that of the NDVI. If performing point to point correlation or analyses of much smaller scales, the different spatial resolutions would have been an issue. However, since the aim was to analyse large scale spatial patterns and make qualitative analyses, the different spatial resolutions of the precipitation data and NDVI data were not an issue.

Initially, it was assumed that the precipitation data did not have a trend during 1981 to 2014 and hence it was not detrended during the data processing. Whether a trend was present was however investigated later. Since no statistically significant trends were revealed for the precipitation during March, April and May it does not have an impact on the results based on this data (Fig. 12). Statistically significant trends were however found for the precipitation during June, July and August and because the construction of EOFs uses data from the entire region, there is a possibility these trends have affected the EOFs of summer precipitation anomalies (Fig. 18). Hence, the results of the summer precipitation have to be interpreted with some caution.

6.2 EOF analysis

6.2.1 Method

During the application of North's rule of thumb it was not clear for neither the spring precipitation anomalies or the summer precipitation anomalies whether the third eigenvalue was distinct from the second and fourth eigenvalues (sections 5.1.1, 5.2.1). The figures of mean NDVI anomalies during anomaly years of PC3, of both spring precipitation anomalies and summer precipitation anomalies, were however excluded from the analyses since they did not provide any meaningful information. This could be an indication that the third eigenvalues were not distinct from the second and fourth eigenvalues, which would mean that only the first and second eigenvalues gave independent physical patterns. This is furthermore indicated by the amount of variance explained by the EOFs since EOF3 of both spring precipitation anomalies and summer precipitation anomalies explains less than 10 % of the variability.

6.2.2 Spatial patterns

The large scale spatial patterns explaining 73.5 % of the precipitation variability in spring and 65,5 % of the precipitation variability in summer were identified for the time period between 1981 to 2014 (Fig. 10, Fig. 16).

The spatial pattern of the first EOF based on spring precipitation anomalies shows coherent, negative anomalies of precipitation along the entire Norwegian coast (Fig. 10). Since the area of anomalous precipitation seems to cover the entire Scandes and the area on the leeward side of these mountains barely show any anomalous precipitation (Fig. 16), this spatial pattern might reflect the results of Uvo (2003), who found that the Scandes are blocking moist Atlantic winds from reaching the Scandinavian inland. Such a prevention

could then be an explanation for the strong precipitation anomalies over the Scandes while weaker anomalies occur over the rest of Scandinavia in EOF1.

The second EOF based on spring precipitation anomalies is very similar to EOF1 based on summer precipitation anomalies (Fig. 10, Fig. 16). The pattern show opposite variations of spring precipitation anomalies along the upper Norwegian coast and over the rest of Scandinavia. This might again be a reflection of the results of Uvo (2003).

Regarding EOF2 based on summer precipitation anomalies, the strong influence the Scandes impose on the Scandinavian precipitation is likely also an explanation for this spatial pattern. The area covers the entire mountain range of the Scandes and so also this spatial pattern seems connected to the blocking of moist Atlantic winds the Scandes exerts (Uvo 2003).

Even though EOF2 of spring precipitation anomalies is similar to EOF1 of summer precipitation anomalies, it is expected that the precipitation variability during spring and summer are different due to the findings of Zveryaev (2006). The reason why the two patterns are nearly identical might be explained through the different geographical domains, since the present study focuses solely on the precipitation variability in Scandinavia while Zveryaev (2006) investigated precipitation variability over Europe.

6.2.3 Comparison of temporal resolutions

The EOFs constructed from yearly spring precipitation anomalies roughly have the same patterns as the ones constructed from monthly spring precipitation anomalies (Fig. 10, Appendix A.4). The differences occur in the strength of the anomalies and how much of the variability the EOFs explain, not in the spatial patterns' configurations. .

The EOFs of yearly summer precipitation anomalies have very similar spatial patterns as the EOFs constructed from monthly summer precipitation anomalies (Fig. 16, Appendix A.8). Some differences are possible to detect, although mainly regarding the strength of the anomalies. Additionally, the spatial patterns of EOF2 has some differences in the extent of coherent variations. These differences are however minor and the patterns principally show similar variations.

A theory for why these smaller differences occur is that there are variations of smaller scale that the yearly precipitation anomalies do not capture since they are averages. The conclusion is drawn that the EOFs of spring precipitation anomalies and summer precipitation anomalies capture roughly the same variability regardless of the temporal resolution of the accumulated precipitation anomalies.

6.3 NDVI analysis

6.3.1 The first principal component

The anomaly years of PC1 based on spring precipitation anomalies did not yield many statistically significant areas of mean NDVI anomalies (Fig. 13). Since EOF1 explains the largest part of the variability of spring precipitation the sparse areas of significant mean NDVI anomalies indicate that spring precipitation modulates very little of summer

vegetation greenness. Additionally, the few statistically significant areas found coincide with areas of low EOF weight, an indication that these are likely due to random variability. As neither of the regional averages of the difference in mean NDVI anomalies between positive and negative anomaly years of PC1 are statistically significant, the weak importance of spring precipitation is further confirmed. However, the difference in mean NDVI anomalies between positive and negative PC1 anomaly years shows a few statistically significant areas of mean NDVI anomalies on the Norwegian coast. These areas overlap with a center of strong negative spring precipitation anomalies in EOF1 (Fig. 10). The difference in mean NDVI anomalies between positive and negative anomaly years essentially shows the difference between unusually dry and wet years. Thus, this area in the middle of the Norwegian coast seems to experience higher productivity during unusually dry springs. This might be due to the fact that vegetation in the Northern Hemisphere mainly is temperature- and radiation limited (Churkina & Runninge 1998; Nemani et al. 2003). Since precipitation often occur during cloud coverage, less radiation might reach the ground when there is excessive precipitation. Thus, there is a possibility that the positive NDVI anomalies occurring during dry springs for PC1 are due to less cloud coverage and more insolation when unusually little precipitation falls, so the limiting growth factor in these areas probably is solar radiation.

The negative anomaly years of PC1 based on summer precipitation anomalies correspond to several statistically significant areas of negative mean NDVI anomalies (Fig. 19). These negative anomaly years imply a variability of summer precipitation of opposite sign configuration than presented for EOF1 (Fig. 16). Thus, when the precipitation anomalies in southern and northeastern Scandinavia are of a negative character, statistically significant negative NDVI anomalies occur in central and northeastern Scandinavia. Additionally, the large statistically significant areas of positive NDVI anomalies of the difference between positive and negative anomaly years of PC1 in central and northeastern Scandinavia implies that the vegetation there has higher productivity during unusually wet summers and thus has a higher carbon uptake (Chapin et al. 2011). Since EOF1 explains the largest part of the variability of summer precipitation the conclusion can be drawn that for summer vegetation in central and northeastern Scandinavia, summer precipitation seems to be of importance. The conclusion is fortified by the regional averages as it is implied that during excessively wet years there are positive statistically significant mean NDVI anomalies. The implication of positive NDVI anomalies during excessive summer precipitation is in accordance with the findings of Smith et al. (2020). The study concluded that during the drought event in Europe the summer 2018, the vegetation productivity decreased in parts of Scandinavia due to less precipitation and low soil moisture. However, both the results of Churkina & Running (1998) and Nemani et al. (2003) show that vegetation in the Northern Hemisphere is predominantly dependent on temperature and radiation, not water availability. The slightly contradicting results may be explained through the different methods as both Churkina & Running (1998) and Nemani et al. (2003) uses modelling approaches whereas the present study investigates actual measurements. The modelling studies might thus capture the predominant signals and dependencies, while the present study indicates that for some smaller areas in Scandinavia summer precipitation is of importance. Additionally, the differences might be due to the present study investigating anomalous years while both Churkina & Running (1998) and Nemani et al. (2003) investigated the annual, overall variability.

6.3.2 The second principal component

The negative anomaly years of PC2 based on spring precipitation anomalies yielded some statistically significant areas of mean NDVI anomalies along the Norwegian coast (Fig. 14). When compared to the spatial pattern of EOF2, the statistically significant areas of PC2 seem to be located on the negative precipitation anomalies, almost along the border between the different signs (Fig. 10). That the statistically significant areas coincide with low EOF2 weight is likely an indication of random variability. Additionally, observation of the difference in mean NDVI anomalies between positive and negative years of PC2 implies that the vegetation along the Norwegian coast has a higher productivity when comparing wet and dry springs. Hence, spring precipitation anomalies along the Norwegian coast does not seem to modulate the vegetation productivity during summer but it is instead affected by other variables. As stated earlier, vegetation growth in the Northern Hemisphere is predominantly limited by temperature and radiation (Churkina & Running 1998; Nemani et al. 2003). Since precipitation often occur during cloud coverage, less radiation might reach the ground when there is excessive precipitation. Thus, there is a possibility that the positive NDVI anomalies occurring during dry springs for PC2 are due to less cloud coverage and more insolation when unusually little precipitation falls. A different theory is that the vegetation in the mountainous areas is not dependent on spring precipitation due to the release of water during snowmelt. According to a study by Löffler (2005) of a small catchment in the mountainous region of central Norway, the snowmelt in a low-alpine belt occurred as late as in June, but as the altitude increased the snow persisted even further into the summer. However, it was found that during snowmelt the ground was too frozen for the water to penetrate, causing most of the meltwater to run past the mountain catchment as surface runoff (Löffler 2005). Hence, the meltwater reaches the vegetation outside the mountainous areas and infiltrate the ground there, providing plenty of soil moisture so the water provided through spring precipitation becomes superfluous.

The anomaly years of PC2 based on summer precipitation anomalies yielded some statistically significant areas of mean NDVI anomalies during both positive and negative anomaly years (Fig. 20). A comparison with EOF2 tells that statistically significant positive NDVI anomalies occur during strong negative summer precipitation anomalies (Fig. 16). It is fortified by the regional average in Norway during PC2 anomaly years which is statistically significant positive during dry years in comparison to wet years. As previously reasoned, this might be because less precipitation often coincides with less cloud coverage and thus more insolation. Therefore, the positive NDVI anomalies during positive PC2 anomaly years could be because of more access to radiation. The statistically significant areas during negative PC2 anomaly years and for the difference between positive and negative anomaly years essentially indicate the same signals. The former shows that negative mean NDVI anomalies in southern and central Scandinavia coincide with EOF2 having weak positive summer precipitation anomalies and the latter shows that during unusually dry years positive NDVI anomalies have occurred in southern and central Scandinavia. The coinciding of negative (positive) NDVI anomalies during positive (negative) summer precipitation anomalies might again be explained through more insolation if there is less precipitation as described above. Additionally, Bastos et al. (2016) concluded that GPP does not show a dependence on soil water during summer in Scandinavia, which is in agreement with these results. Thus, the summer precipitation

anomalies during PC2 anomaly years does not seem to have such a strong impact on the summer vegetation greenness.

6.3.3 Comparison of temporal resolutions

When comparing the monthly mean NDVI anomalies during PC anomaly months with the yearly mean NDVI anomalies during PC anomaly years for both the spring- and summer data sets, differences can be observed (Fig. 13, Fig. 14, 19, 20, Appendix A.1, A.2, A.6, A.10). Generally, it is notable that there are vast areas of zero monthly mean NDVI anomalies during PC anomaly months, primarily along the Norwegian coast. These zero monthly mean NDVI anomalies are not as present in the yearly mean NDVI anomalies. Additionally, some areas nearly have the opposite signs between the monthly mean NDVI anomalies and the yearly mean NDVI anomalies, e.g. the yearly mean NDVI anomalies during negative PC2 anomaly years of spring precipitation anomalies and the monthly mean NDVI anomalies during negative PC2 anomaly months of spring precipitation anomalies (Fig. 14, Appendix A.6). However, there seems to be a larger occurrence of statistically significant yearly mean NDVI anomalies during PC anomaly years than during PC anomaly months. Because not as strong signals are produced for the monthly mean NDVI anomalies, a hypothesis for the different results due to the different temporal resolutions is that the seasonal- and interannual variability is mixed for the mean monthly NDVI anomalies and this is why there are much less areas of statistically significance for these means.

6.4 Teleconnection analysis

The teleconnection analysis was only performed for the summer precipitation and not for the spring precipitation. The present study initially focused on summer precipitation in Scandinavia, its potential relation with summer vegetation in the same area and through this whether a connection could be found to the dominant weather regimes. Thus, the present study did not include spring precipitation in the beginning and so the summer precipitation was of more importance. Additionally, when spring precipitation was included in the present study, the teleconnection analysis was not performed with spring precipitation because of the limited time.

Due to the time constraint of the present study, it was not investigated whether the data were normally distributed or not and it was therefore assumed to be so in order to apply Pearson's correlation test. Since the distributions of the data were not known, Pearson's correlation test might not be an appropriate choice which could affect the resulting found correlations.

6.4.1 The first principal component

Both SNAO and EA are found to have statistically significant correlations to PC1 where SNAO has the strongest correlation of the investigated combinations (Table 3). The R indicates that when the SNAO is in its negative phase, the sign configuration shown of the spatial pattern of EOF1 is similar to the precipitation variability, i.e. negative precipitation anomalies along the Norwegian coast and positive precipitation anomalies in southern Scandinavia and the entire inland (Fig. 16). The relation is expected since negative phases of the SNAO have been found to provide wet conditions in northern

Europe (Boé et al. 2009; Folland et al. 2009). Additionally, the small area along the northern Norwegian coast of opposite sign to the precipitation variability in southern and western Scandinavia might reflect the results of Zveryaev (2004) which states that northeastern Scandinavia receives more precipitation during positive phases of the SNAO.

The conclusion is drawn that there is a relation between the summer precipitation patterns and the SNAO. The negative correlation between SNAO and PC1 is further related to the NDVI analysis as negative mean NDVI anomalies seem to occur when EOF1 has a sign configuration opposite to the one shown of the spatial pattern. Thus, the conclusion is drawn that a positive SNAO coincides with decreased summer vegetation greenness in the central Scandinavian inland.

The correlation between PC1 and the EA index is not as strong as for PC1 and the SNAO index. The correlation indicates that positive anomaly years occur mainly during positive EA phases and vice versa (Fig. 21). According to the findings of Boé et al. (2007), the AR affects the summer precipitation in northern Europe as it provides wetter conditions than normal. Since the EA has a strong resemblance to the AR (Hurrell & Deser 2010; Moore et al. 2013), the above-mentioned influence of the AR can be assumed to resemble the influence that the EA has on precipitation in the same region. The assumption is somewhat confirmed as Wibig (1999) found that the EA has a positive correlation with precipitation in northern Europe, however during winter. The positive correlation found in the present study between PC1 and the EA index indicates that the positive phase of the EA matches the positive configuration of EOF1, and both of these patterns correspond to wetter conditions in the majority of Scandinavia (Fig. 16).

Since the EA has a positive correlation with PC1, the results from the NDVI analysis can be interpreted as during negative EA phases, the opposite sign configuration than shown of EOF1 resembles the variability of summer precipitation anomalies. Thus, negative EA phases coincides with decreased summer vegetation greenness in the central Scandinavian inland. The conclusion drawn from this is that the EA has a relation to the summer precipitation patterns which implies it has an effect on the summer vegetation greenness in the central Scandinavian inland.

6.4.2 The second principal component

The anomaly years of PC2 do not show any clear correlation with either the SNAO or EA index (Table 3). However, there is a statistically significant positive correlation between the SCA index and PC2 so during positive phases of the SCA, the summer precipitation anomalies are negative along the Norwegian coast and northern Scandinavia. This is somewhat concordant with the results of Jaagus (2009), who found that during winter the positive phase of SCA causes decreased precipitation over the Scandes, over which the anomaly center occurs for EOF2.

The positive correlation between PC2 and SCA means that there is a relation between the summer precipitation pattern of EOF2 and the SCA. For summer vegetation greenness this implies that during positive phases of the SCA, there is a negative summer precipitation variability which coincides with positive summer vegetation greenness along the Scandes.

7 Conclusions and future perspectives

The large scale spatial patterns which explain the precipitation variability over Scandinavia between 1981 to 2014 have been identified for both precipitation anomalies during spring and during summer. Based on these patterns, the conclusion can be drawn that the Scandes seem to be of importance for the precipitation variability in this region. This is based on the fact that these mountainous areas are clearly visible in the spatial patterns which constitute the bulk of the variability. It can also be concluded that there are similarities between the spatial patterns of precipitation variability during spring and summer.

With regard to the spring precipitation variability and how it affects summer vegetation greenness, it seems to have very little impact and thus not have such a strong, lagged connection to the terrestrial C-cycle. The summer precipitation variability on the other hand is indicated to modulate some of the summer vegetation greenness in central- and northeastern Scandinavia. However, indications of several negative relations between precipitation variability and summer vegetation greenness are also detected which implies that other variables such as radiation or temperature are of more importance.

Statistically significant correlations are found between a large portion of the patterns of summer precipitation variability and the SNAO and EA teleconnection patterns. Thus, the SNAO and EA affect summer precipitation variability which implies they have an impact on the summer vegetation greenness. A correlation was also found between SCA and a smaller portion of the patterns of summer precipitation variability.

Future improvements of the study would first and foremost be to perform the same study again but detrend the precipitation data to avoid the trend affecting the results. The analyses would also be improved by investigating the distributions of the summer precipitation and the teleconnection indices, to ensure a suitable correlation test is applied. Another improvement would be to use the method of REOFs instead of EOFs to make direct physical interpretations possible. The study could furthermore be developed by making point correlations between the precipitation anomalies and the summer vegetation greenness. This would give numerical values and significance of the relations, thus providing more certain results of the roles of spring and summer precipitation variability. It would additionally be interesting to analyse the relation between spring precipitation variability and spring vegetation greenness since it could provide further insight of eventual lagged effects and how the signals of spring vegetation extends into summer. To obtain even more information regarding the relation between the precipitation variability and teleconnections, an analysis of the relation between precipitation variability and SLP might provide more insight since the teleconnections are commonly defined through SLP.

References

Atmospheric flow Analogues for Climate Change (n.d.). *MAM Weather regimes.* https://a2c2.lsce.ipsl.fr/index.php/78-main-menu/104-mam-weather-regimes [2021-05-19]

Barnston, A.G. & Livezey, R.E. (1987). Classification, Seasonality and Persistence of Low-Frequency Atmospheric Circulation Patterns. *Monthly Weather Review.* 115, 1083-1126. https://doi.org/10.1175/1520-0493(1987)115<1083:CSAPOL>2.0.CO;2

Bastos, A., Janssens, I.A., Gouveia, C.M., Trigo, R.M., Ciais, P., Chevallier, F., Peñuelas, J., Rödenbeck, C., Piao, S., Friedlingstein, P. & Running, S.W. (2016). European land CO_2 sink influenced by NAO and East-Atlantic Pattern coupling. *Nature Communications.* 7, 10315. https://doi.org/10.1038/ncomms10315

Boé, J., Terray, L., Cassou, C. & Najac, J. (2009). Uncertainties in European summer precipitation changes: role of large scale circulation. *Climate Dynamics.* 33, 265-276. https://doi.org/10.1007/s00382-008-0474-7

Cassou, C. (2008). Intraseasonal interaction between the Madden-Julian Oscillation and the North Atlantic Oscillation. *Nature.* 455, 523-527. https://doi.org/10.1038/nature07286

Cassou, C., Terray, L. & Phillips, A.S. (2005). Tropical Atlantic Influence on European Heat Waves. *Journal of Climate.* 18, 2805-2811. https://doi.org/10.1175/JCLI3506.1

Cassou, C., Terray, L., Hurrell, J.W. & Deser, C. (2004). North Atlantic Winter Climate Regimes: Spatial Asymmetry, Stationarity with Time, and Oceanic Forcing. *Journal of Climate.* 17, 1055-1068. https://doi.org/10.1175/1520-0442(2004)017<1055:NAWCRS>2.0.CO;2

Chapin, F.S., Matson, P.A. & Vitousek, P.M. (2011). *Principles of Terrestrial Ecosystem Ecology.* 2a uppl., New York: Springer Science+Buisness Media.

Churkina, G. & Running, S.W. (1998). Contrasting Climatic Controls on the Estimated Productivity of Global Terrestrial Biomes. *Ecosystems.* 1, 206-215. https://www.jstor.org/stable/3658588

Ciais, P., Sabine, C., Bala, g., Bopp, L., Brovkin, V., Canadell, J., Chhabra, A., DeFries, R., Galloway, J., Heimann, M., Jones, C., Le Quéré, C., Myneni, R.B., Piao, S. & Thornton, P. (2013). Carbon and Other Biogeochemical Cycles. I: Stocker, T.F., Qin, D., Plattner, G.-K., Tignor, M., Allen, S.K., Boschung, J., Nauels, A., Xia, Y., Bex, V. & Midgley, P.M. (eds.) *Climate Change 2013: The Physical Science Basis. Contribution of Working Group I to the Fifth Assessment Report of the Intergovernmental Panel on Climate Change.* Cambridge, United Kingdom and New York, NY, USA: Cambridge University Press. 465-570.

Defries, R.S. & Townshend, J.R.G. (1994). NDVI-Derived Land Cover Classification at a Global Scale. *International Journal of Remote Sensing.* 15, 3567-3586. https://doi.org/10.1080/01431169408954345

Eastman, J.R., Sangermano, F., Machado, E.A., Rogan, J. & Anyamba, A. (2013). Global Trends in Seasonality of Normalized Difference Vegetation Index (NDVI), 1982-2011. *Remote Sensing.* 5, 4799-4818. https://doi.org/10.3390/rs5104799

Fabiano, F., Christensen, H.M., Strommen, K., Athanasiadis, P., Baker, A., Schiemann, R. & Corti, S. (2020). Euro-Atlantic weather Regimes in the PRIMAVERA coupled climate simulations: impact of resolution and mean state biases on model performance. *Climate Dynamics.* 54, 5031-5048. https://doi.org/10.1007/s00382-020-05271-w

Fil, C. & Dubus, L. (2005). Winter climate regimes over the North Atlantic and European region in ERA40 reanalysis and DEMETER seasonal hindcasts. *Tellus A: Dynamic Meteorology and Oceanography.* 57, 290-307. https://doi.org/10.3402/tellusa.v57i3.14671

Folland, C.K., Knight, J., Linderholm, H.W., Fereday, D., Ineson, S. & Hurrell, J.W. (2009). The Summer North Atlantic Oscillation: Past, Present, and Future. *American Meteorological Society.* 22, 1082-1103. https://doi.org/10.1175/2008JCLI2459.1

Frank, D., Reichstein, M., Bahn, M., Thonicke, K., Frank, D., Mahecha, M.D., Smith, P., Van der Velde, M., Vicca, S., Babst, F., Beer, C., Buchmann, N., Canadell, J.G., Ciais, P., Cramer, W., Ibrom, A., Miglietta, F., Poulter, B., Rammig, A., Seneviratne, S.I., Walz, A., Wattenbach, M., Zavala, M.A. & Zscheischler, J. (2015). Effects of climate extremes on the terrestrial carbon cycle: concepts, processes and potential future impacts. *Global Change Biology.* 21, 2861-2880. https://doi.org/10.1111/gcb.12916

Gong, D.-Y. & Ho, C.-H. (2003). Detection of large-scale climate signal in spring vegetation index (normalized difference vegetation index) over the Northern Hemisphere. *Journal of Geophysical Research.* 108, 4498. https://doi.org/10.1029/2002JD002300

Gonsamo, A., Chen, J.M. & Lombardozzi, D. (2016). Global vegetation productivity response to climatic oscillations during the satellite era. *Global Change Biology.* 22, 3414-3426. https://doi.org/10.1111/gcb.13258

Gouveia, C., Trigo, R.M., DaCamara, C.C, Libonati, R. & Pereira, J.M.C. (2008). The North Atlantic Oscillation and European vegetation dynamics. *International Journal of Climatology.* 28, 1835-1847. https://doi.org/10.1002/joc.1682

Goward, S.N., Tucker, C.J. & Dye, D.G. (1985). North American Vegetation Patterns Observed with the NOAA-7 Advanced Very High Resolution Radiometer.

Vegetatio. 64, 3-14. https://www.jstor.org/stable/20037229

Guemas, V., Salas-Mélia, D., Kageyama, M., Giordani, H., Voldoire, A. & Sanchez-Gomez, E. (2010). Summer interactions between weather regimes and surface ocean in the North-Atlantic region. *Climate Dynamics.* 34, 527-546. https://doi.org/10.1007/s00382-008-0491-6

Hannachi, A. (2004). A primer for EOF analysis of climate data. Department of Meteorology, University of Reading, U.K. https://www.researchgate.net/publication/228781584_A_primer_for_EOF_analysis_of_climate_data

Hannachi, A., Jolliffe, T. & Stephenson, D.B. (2007). Empirical orthogonal functions and related techniques in atmospheric science: A review. *International Journal of Climatology.* 27, 1119-1152. https://doi.org/10.1002/joc.1499

Hersbach, H., Bell, B., Berrisford, P., Hirahara, S., Horányi, A., Muñoz-Sabater, J., Nicolas, J., Peubey, C., Radu, R., Schepers, D., Simmons, A., Soci, C., Abdalla, S., Abellan, X., Balsamo, G., Bechtold, P., Biavati, G., Bidlot, J., Bonavita, M., De Chiara, G., Dahlgren, P., Dee, D., Diamantakis, M., Dragani, R., Flemming, J., Forbes, R., Fuentes, M., Geer, A., Haimberger, L., Healy, S., Hogan, R.J., Hólm, E., Janisková, M., Keeley, S., Laloyaux, P., Lopez, P., Lupu, C., Radnoti, G., de Rosnay, P., Rozum, I., Vamborg, F., Villaume, S. & Thépaut, J.-N. (2020). The ERA5 global reanalysis. *Quarterly Journal of the Royal Meteorological Society.* 146, 1999-2049. https://doi.org/10.1002/qj.3803

Hurrell, J.W. (1995). Decadal Trends in the North Atlantic Oscillation: Regional Temperatures and Precipitation. *Science.* 269, 676-679. https://www.jstor.org/stable/2888966

Hurrell, J.W. & Deser, C. (2010). North Atlantic climate variability: The role of the North Atlantic Oscillation. *Journal of Marine Systems.* 79, 231-244. https://doi.org/10.1016/j.jmarsys.2008.11.026

Jaagus, J. (2009). Regionalisation of the precipitation pattern in the Baltic Sea drainage basin and its dependence on large-scale atmospheric circulation. *Boreal Environment Research.* 14, 31-44. http://hdl.handle.net/10138/233255

Kottek, M., Grieser, J., Beck, C., Rudolf, B. & Rubel, F. (2006). World Map of the Köppen-Geiger climate classification updated. *Meteorologische Zeitschrift.* 15, 259-263. https://doi.org/10.1127/0941-2948/2006/0130

Li, J., Fan, K. & Xu, Z. (2016). Links between the late wintertime North Atlantic Oscillation and springtime vegetation growth over Eurasia. *Climate Dynamics.* 46, 987-1000. https://doi.org/10.1007/s00382-015-2627-9

Löffler, J. (2005). Snow cover dynamics, soil moisture variability and vegetation ecology in high mountain catchments of central Norway. *Hydrological Processes.* 19, 2385-2405. https://doi.org/10.1002/hyp.5891

Messori, G., Ruiz-Pérez, G., Manzoni, S. & Vico, G. (2019). Climate drivers of the terrestrial carbon cycle variability in Europe. *Environmental Research Letters.* 14, 063001. https://doi.org/10.1088/1748-9326/ab1ac0

Michelangeli, P.-A., Vautard, R. & Legras, B. (1995). Weather Regimes: Recurrence and Quasi Stationarity. *Journal of the Atmospheric Sciences.* 52, 1237-1256. https://doi.org/10.1175/1520-0469(1995)052<1237:WRRAQS>2.0.CO;2

Moore, G.W.K., Renfrew, I.A. & Pickart, R.S. (2013). Multidecadal Mobility of the North Atlantic Oscillation. *Journal of Climate.* 26, 2453-2466. https://doi.org/10.1175/JCLI-D-12-00023.1

Mukougawa, H. & Sato, H. (1999). Multiple Weather Regimes in the Summertime North Atlantic Circulation. *Journal of the Meteorological Society of Japan.* 77, 483-494. https://doi.org/10.2151/jmsj1965.77.2_483

Myneni, R.B., Keeling, C.D., Tucker, C.J., Asrar, G. & Nemani, R.R. (1997). Increased plant growth in the northern high latitudes from 1981 to 1991. *Nature.* 386, 698-702. https://doi.org/10.1038/386698a0

NASA (2011). *The Carbon Cycle.* https://earthobservatory.nasa.gov/features/CarbonCycle [2021-03-23]

Nemani, R.R., Keeling, C.D., Hashimoto, H., Jolly, W.M., Piper, S.C., Tucker, C.J., Myneni, R.B. & Running, S.W. (2003). Climate-Driven Increases in Global Terrestrial Net Primary Production from 1982 to 1999. *Science.* 300, 1560-1563. https://doi.org/10.1126/science.1082750

NOAA National Weather Service Climate Prediction Center (2012). *Northern Hemisphere Teleconnection Patterns.* https://www.cpc.ncep.noaa.gov/data/teledoc/telecontents.shtml [2021-03-09]

NOAA National Weather Service Climate Prediction Center (2005). *East Atlantic.* https://www.cpc.ncep.noaa.gov/data/teledoc/ea_map.shtml [2021-04-08]

North, G.R., Bell, T.L., Cahalan, R.F. Moeng, F.J. (1982). Sampling Errors in the Estimation of Empirical Orthogonal Functions. *Monthly Weather Review.* 7, 699-706. https://doi.org/10.1175/1520-0493(1982)110<0699:SEITEO>2.0.CO;2

Piao, S., Wang, X., Wang, K., Li, X., Bastos, A., Canadell, J.G., Ciais, P., Friedlingstein, P. & Sitch, S. (2019). Interannual variation of terrestrial carbon cycle: Issues and perspectives. *Global Change Biology.* 26, 300-318. https://doi.org/10.1111/gcb.14884

Rasmusson, E.M. & Wallace, J.M. (1983). Meteorological Aspects of the El Niño/Southern Oscillation. *Science.* 222, 1195-1202. https://doi.org/10.1126/science.222.4629.1195

Reichstein, M., Bahn, M., Ciais, P., Frank, D., Mahecha, M.D., Seneviratne, S.I., Zscheischler, J., Beer, C., Buchmann, N., Frank, D.C., Papale, D., Rammig, A., Smith, P., Thonicke, K., van der Velde, M., Vicca, S., Walz, A. & Wattenbach, M. (2013). Climate extremes and the carbon cycle. *Nature.* 500, 287-295. https://doi.org/10.1038/nature12350

Reichstein, M., Ciais, P., Papale, D., Valentini, R., Running, S., Viovy, N., Cramer, W., Granier, A., Ogée, J., Allard, V., Aubinet, M., Bernhofer, Chr., Buchmann, N., Carrara, A., Grünwald, T., Heimann, M., Heinesch, B., Knohl, A., Kutsch, W., Loustau, D., Manca, G., Matteucci, G., Miglietta, F., Ourcival, J.M., Pilegaard, K., Pumpanen, J., Rambal, S., Schaphoff, S., Seufert, G., Soussana, J.-F., Sanz, M.-J., Vesala, T. & Zhao, M. (2007). Reduction of ecosystem productivity and respiration during the European summer 2003 climate anomaly: a joint flux tower, remote sensing and modelling analysis. *Global Change Biology.* 13, 634-651. https://doi.org/10.1111/j.1365-2486.2006.01224.x

Schlining, B., Crosby, A. & Signell, R. (2013). NCTOOLBOX.

Seneviratne, S.I., Nicholls, N., Easterling, D., Goodess, C.M., Kanae, S., Kossin, J., Luo, Y., Marengo, J., McInnes, K., Rahimi, M., Reichstein, M., Sorteberg, A., Vera, C. & Zhang, X. (2012). Changes in climate extremes and their impacts on the natural physical environment. I: Field, C.B., Barros, V., Stocker, T.F., Qin, D., Dokken, D.J., Ebi, K.L., Mastrandrea, M.D., Mach, K.J., Plattner, G.-K., Allen, S.K., Tignor, M. & Midgley, P.M. (eds). *Managing the Risks of Extreme Events and Disasters to Advance Climate Change Adaption. A Special Report of Working Groups I and II of the Intergovernmental Panel on Climate Change (IPCC).* Cambridge, United Kingdom and New York, NY, YSA: Cambridge University Press. 109-230.

Smith, N.E., Kooijmans, L.M.J., Koren, G., van Schaik, E., van der Woude, A.M., Wanders, N., Ramonet, M., Xueref-Remy, I., Siebicke, L., Manca, G., Brümmer, C., Baker, I.T., Haynes, K.D., Luijkx, I.T. & Peters, W. (2020). Spring enhancement and summer reduction in carbon uptake during the 2018 drought in northwestern Europe. *Philosophical Transactions of the Royal Society B.* 375. http://dx.doi.org/10.1098/rstb.2019.0509

Tucker, C.J. (1979). Red and Photographic Infrared Linear Combinations for Monitoring Vegetation. *Remote Sensing of Environment.* 8, 127-150. https://www.sciencedirect.com/science/article/abs/pii/0034425779900130

Uvo, C.B. (2003). Analysis and regionalization of northern European winter precipitation based on its relationship with the North Atlantic oscillation. *International Journal of Climatology.* 23, 1185-1194. https://doi.org/10.1002/joc.930

Vautard, R. (1990). Multiple Weather Regimes over the North Atlantic: Analysis of Precursors and Successors. *Monthly Weather Review.* 118, 2056-2081. https://doi.org/10.1175/1520-0493(1990)118<2056:MWROTN>2.0.CO;2

von Buttlar, J., Zscheischler, J., Rammig, A., Sippel, S., Reichstein, M., Knohl, A., Jung, M., Menzer, O., Altaf Arain, M., Buchmann, N., Cescatti, A., Gianelle, D., Kiely, G., Law, B.E., Magliulo, V., Margolis, H., McCaughey, H., Merbold, L., Migliavacca, M., Montagnani, L., Oechel, W., Pavelka, M., Peichl, M., Rambal, S., Raschi, A., Scott, R.L., Vaccari, F.P., van Gorsel, E., Varlagin, A., Wohlfahrt, G. & Mahecha, M.D. (2018). Impacts of droughts and extreme-temperature events on gross primary production and ecosystem respiration: a systematic assessment across ecosystems and climate zones. *Biogeosciences.* 15, 1293-1318. doi.org/10.5194/bg-15-1293-2018

Wallace, J.M. & Gutzler, D.S. (1981). Teleconnections in the Geopotential Height Field during the Northern Hemisphere Winter. *Monthly Weather Review.* 109, 784-812. https://doi.org/10.1175/1520-0493(1981)109<0784:TITGHF>2.0.CO;2

Wang, M. & Tan, B. (2020). Two Types of the Scandinavian Pattern: Their Formation Mechanisms and Climate Impacts. *Journal of Climate.* 33, 2645-2661. https://doi.org/10.1175/JCLI-D-19-0447.1

Wang, Q., Tenhunen, J., Dinh, N.Q., Reichstein, M., Vesala, T. & Keronen, P. (2004). Similarities in ground- and satellite-based NDVI time series and their relationship to physiological activity of a Scots pine forest in Finland. *Remote Sensing of Environment.* 93, 225-237. https://doi.org/10.1016/j.rse.2004.07.006

Wibig, J. (1999). Precipitation in Europe in relation to circulation patterns at the 500 hPa level. *International Journal of Climatology.* 19, 253-269. https://doi.org/10.1002/(SICI)1097-0088(19990315)19:3<253::AID-JOC366>3.0.CO;2-0

Wu, M., Vico, G., Manzoni, S., Cai, Z., Bassiouni, M., Tian, F., Zhang, J., Ye, K. & Messori, G. (2021). Early growing season anomalies in vegetation activity determine the large-scale climate-vegetation coupling in Europe. *Journal of Geophysical Research: Biogeosciences.* 126. https://doi.org/10.1029/2020JG006167

Zhou, L., Tucker, C.J., Kaufmann, R.K., Slayback, D., Shabanov, N.V. & Myneni, R.B. (2001). Variations in northern vegetation activity inferred from satellite data of vegetation index during 1981 to 1999. *Journal of Geophysical Research.* 106, 20 069-20 083. https://doi.org/10.1029/2000JD000115

Zveryaev, I.I. (2004). Seasonality in precipitation variability over Europe. *Journal of Geophysical Research.* 109, D05103. https://doi.org/10.1029/2003JD003668

Zveryaev, I.I. (2006). Seasonally varying modes in long-term variability of European precipitation during the 20th century. *Journal of Geophysical Research.* 111, D21116. https://doi.org/10.1029/2005JD006821

Ågren, G. & Andersson, F. (2012). *Terrestrial ecosystem ecology: principles and applications.* United Kingdom, Cambridge: Cambridge University Press.

A Appendix

A.1 Results from analysis of the third EOF based on yearly spring precipitation anomalies

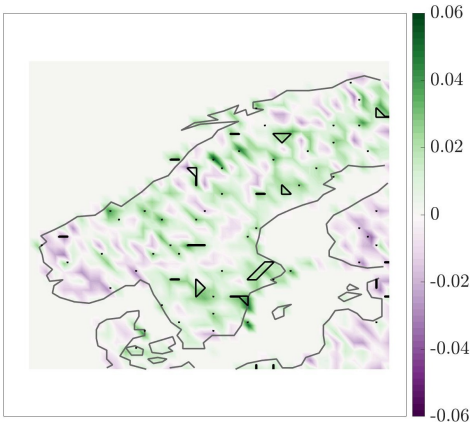

(a) Mean yearly summer NDVI anomalies during positive PC3 anomaly years.

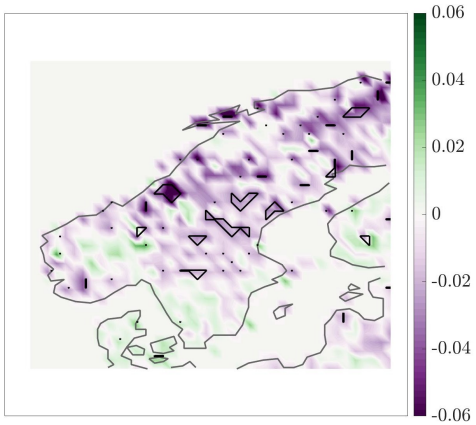

(b) Mean yearly summer NDVI anomalies during negative PC3 anomaly years.

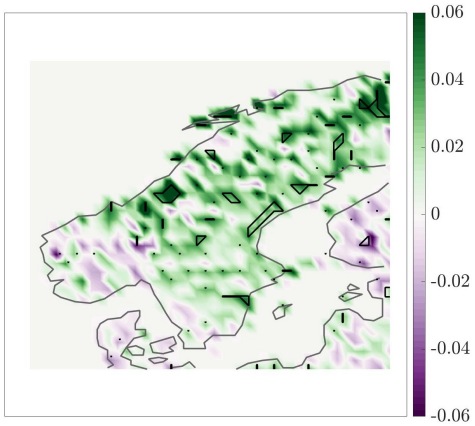

(c) The difference in mean yearly summer NDVI anomalies between positive and negative PC3 anomaly years.

Figure I: Mean yearly summer NDVI anomalies during anomaly years of the third principal component (PC3) of yearly accumulated precipitation anomalies in March, April and May in Scandinavia 1981 to 2014. Statistically significant anomalies at the 90 % level are encircled by black lines. The NDVI anomalies are based on yearly averages of NDVI in June, July and August in Scandinavia 1981 to 2014.

Table I: Regional average of the difference in mean yearly summer NDVI anomalies between positive and negative anomaly years for the third principal component. Statistically significant values are marked with * at the 90 % level.

	Mean yearly summer NDVI anomaly
Southern Scandinavia	0.0057
Central- and northeastern Sweden	0.022*
Norway	0.023*

A.2 Results from analysis of the third EOF based on yearly summer precipitation anomalies

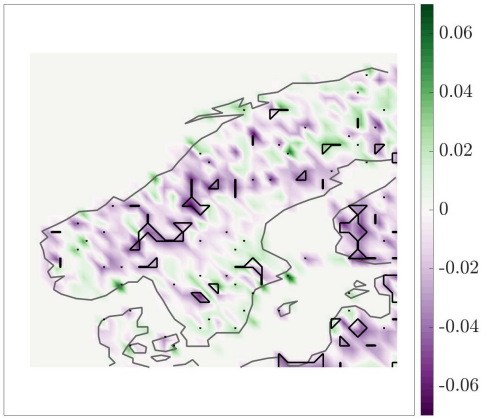

(a) Mean yearly summer NDVI anomalies during positive PC3 anomaly years.

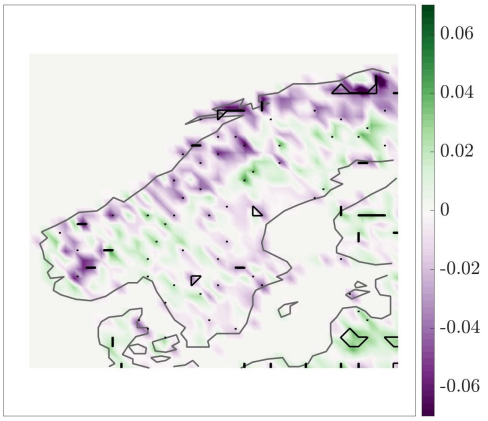

(b) Mean yearly summer NDVI anomalies during negative PC3 anomaly years.

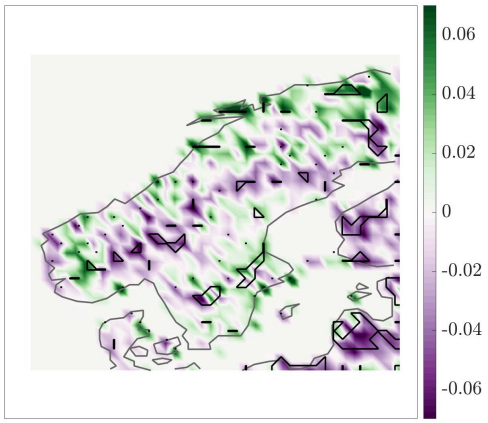

(c) The difference in mean yearly summer NDVI anomalies of positive and negative PC3 anomaly years.

Figure II: Mean yearly summer NDVI anomalies during anomaly years of the third principal component (PC3) of yearly accumulated precipitation anomalies in June, July and August in Scandinavia 1981 to 2014. Statistically significant anomalies at the 90 % level are encircled by black lines. The NDVI anomalies are based on yearly averages of NDVI in June, July and August in Scandinavia 1981 to 2014.

Table II: Regional average of the difference in mean yearly summer NDVI anomalies between positive and negative anomaly years for the third principal component. None of the anomalies are statistically significant at the 90 % level.

	Mean yearly summer NDVI anomaly
Southern Scandinavia	-0.00043
Central- and northeastern Sweden	-0.0028
Norway	0.0084

Table III: The correlation between the yearly average index, solely based on June, July and August, of the Summer North Atlantic Oscillation (SNAO), the East Atlantic pattern (EA) and the Scandinavian pattern (SCA) 1981 to 2014 and the third principal component (PC3). None of the anomalies are statistically significant at the 95 % level.

	Teleconnection index	R-value
PC3	SNAO	0.081
	EA	0.23
	SCA	0.23

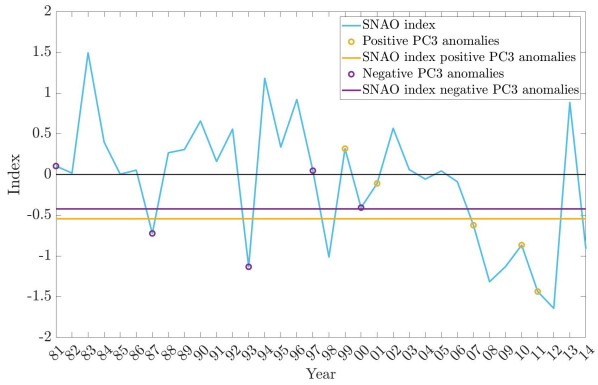

(a) SNAO index with PC3 anomaly years marked.

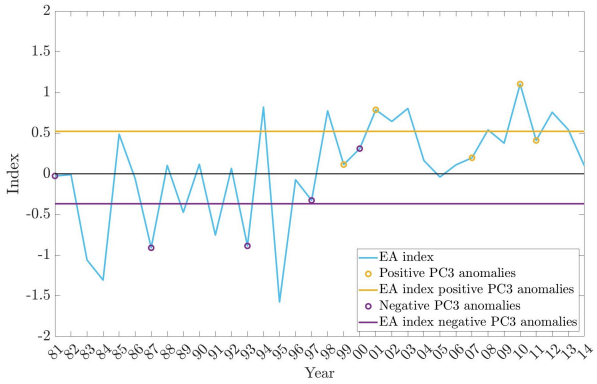

(b) EA index with PC3 anomaly years marked.

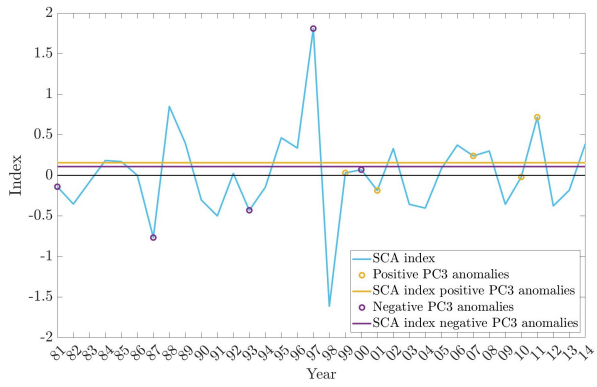

(c) SCA index with PC3 anomaly years marked.

Figure III: The yearly average index, solely based on June, July and August, of the Summer North Atlantic Oscillation (SNAO), the East Atlantic pattern (EA) and the Scandinavian pattern (SCA) 1981 to 2014. The positive and the negative anomaly years of the third principal component (PC3) are marked. Additionally, the average value of the index during the positive an the negative years respectively is marked, to indicate if there is a tendency to a certain configuration of the teleconnection patterns during the years of anomalous precipitation. The PC is based on anomalies of the yearly accumulated precipitation in June, July and August.

A.3 North's rule of thumb based on monthly spring precipitation anomalies

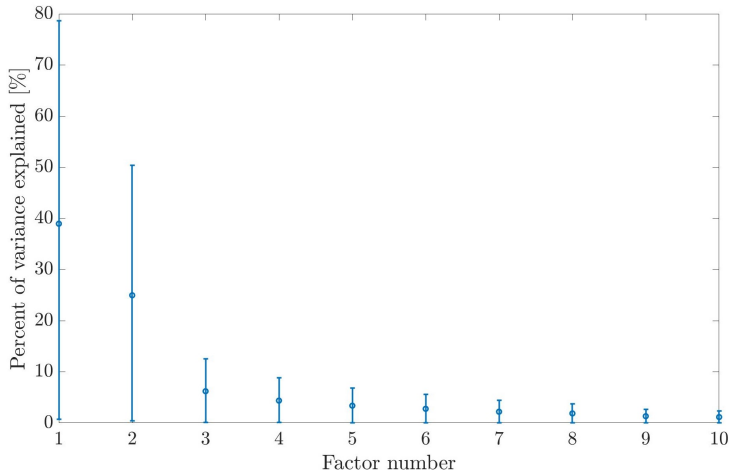

Figure IV: The percent of variance explained by the first ten eigenvalues of mean monthly spring precipitation anomalies, with the associated sampling errors. The three first eigenvalues were determined to be distinct through the application of North's rule of thumb (North et al. 1982).

A.4 Spatial pattern of the EOFs based on monthly spring precipitation anomalies

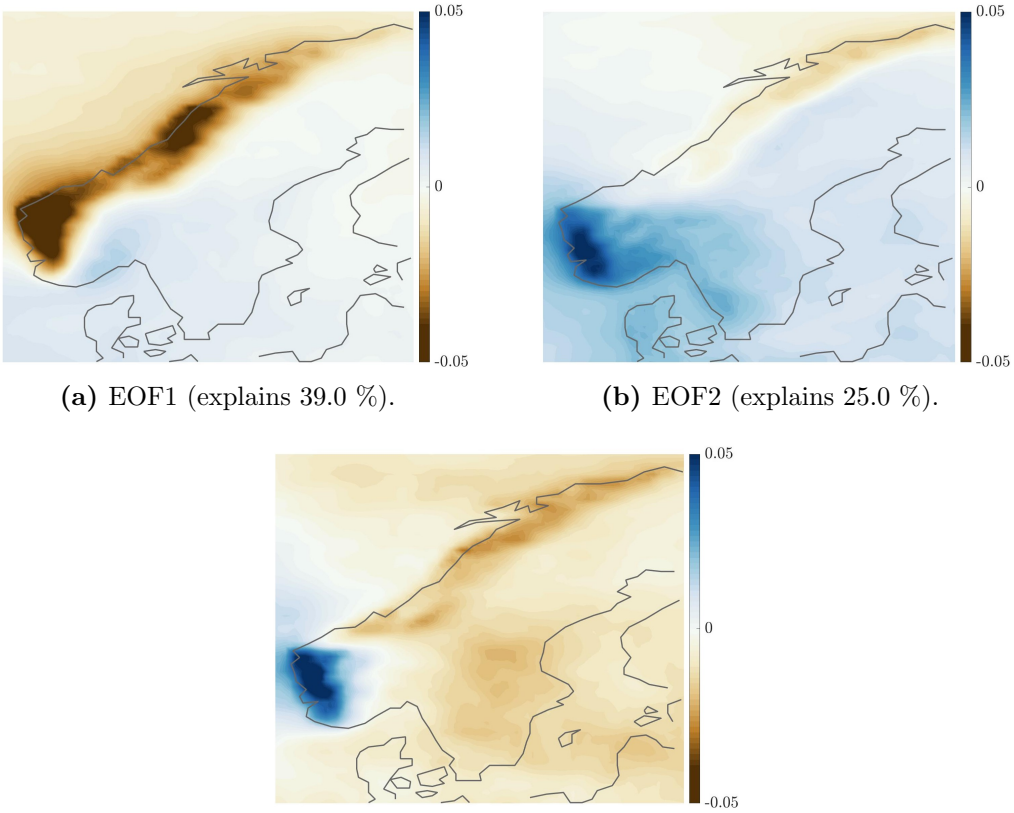

(a) EOF1 (explains 39.0 %).

(b) EOF2 (explains 25.0 %).

(c) EOF3 (explains 6.21 %).

Figure V: Spatial patterns of the first three empirical orthogonal functions (EOFs) chosen for analysis. The spatial patterns show the variability of mean monthly spring precipitation, based on cumulative precipitation in March, April and May in Scandinavia 1981 to 2014. The colorbar shows the precipitation anomalies in mm/month.

A.5 Principal components based on monthly spring precipitation anomalies

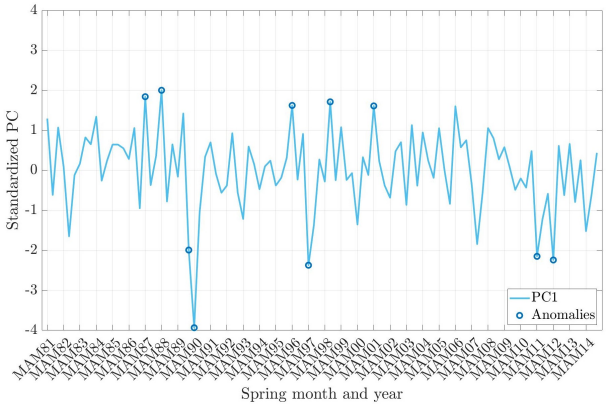

(a) Standardized PC1.

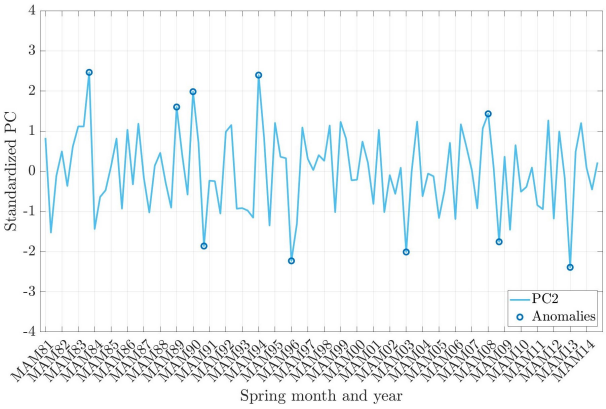

(b) Standardized PC2.

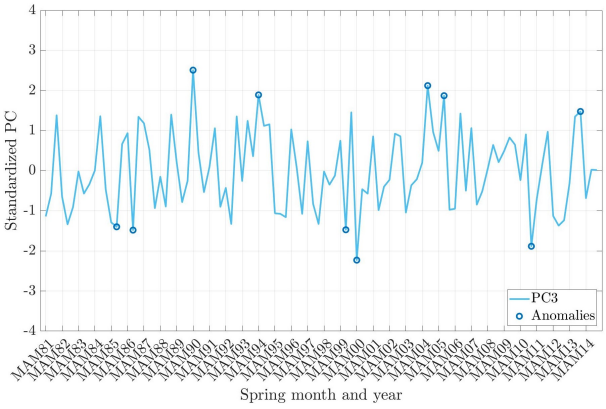

(c) Standardized PC3.

Figure VI: Standardized principal components (PCs) corresponding to the first three empirical orthogonal functions (EOFs) of monthly spring precipitation anomalies. The mean anomalies are based on the cumulative precipitation in March, April and May in Scandinavia 1981 to 2014. The ticks of the x-axis lie on the point of March each year, thus the two points in the graph following each x-axis tick are April and May each year. For each PC the five largest and the five lowest values are marked, showing months of anomalous precipitation variability.

A.6 Monthly summer NDVI anomalies for the principal components of monthly spring precipitation anomalies

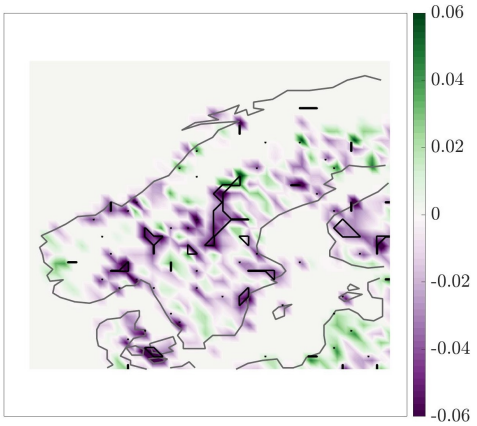

(a) Mean monthly summer NDVI anomalies during positive PC1 anomaly months.

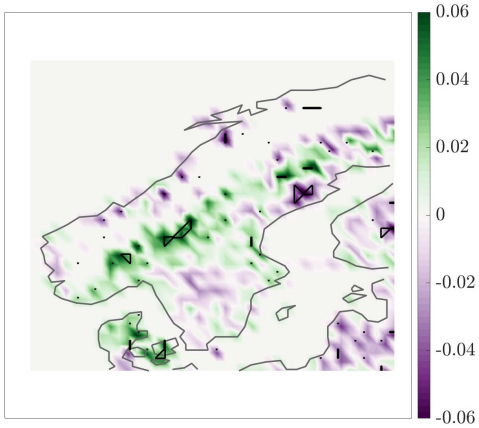

(b) Mean monthly summer NDVI anomalies during negative PC1 anomaly months.

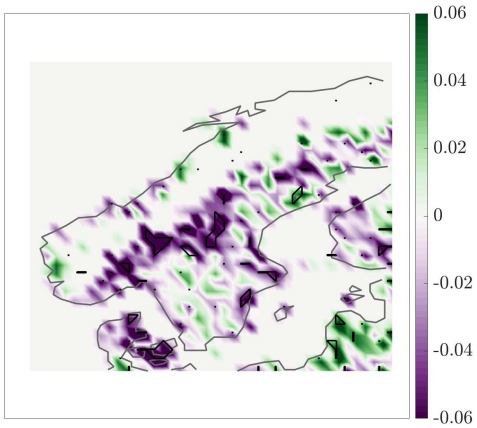

(c) The difference in mean monthly summer NDVI anomalies between positive and negative PC1 anomaly months.

Figure VII: Mean monthly summer NDVI anomalies during anomaly months of the first principal component (PC1) of monthly accumulated precipitation anomalies in March, April and May in Scandinavia 1981 to 2014. Statistically significant anomalies at the 90 % level are encircled by black lines. The NDVI anomalies are based on monthly averages of NDVI in June, July and August respectively in Scandinavia 1981 to 2014.

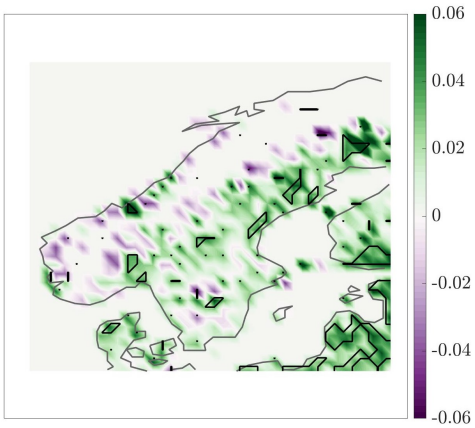

(a) Mean monthly summer NDVI anomalies during positive PC2 anomaly months.

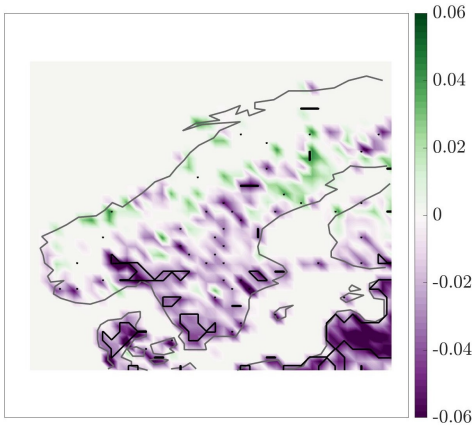

(b) Mean monthly summer NDVI anomalies during negative PC2 anomaly months.

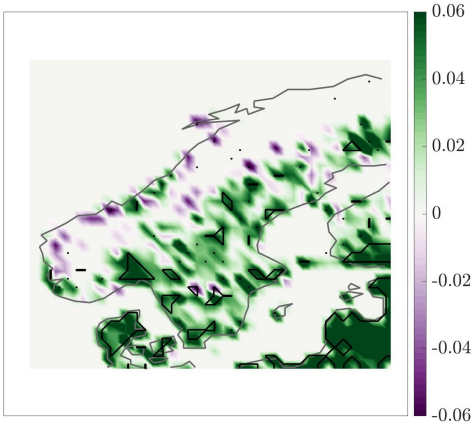

(c) The difference in mean monthly summer NDVI anomalies between positive and negative PC2 anomaly months.

Figure VIII: Mean monthly summer NDVI anomalies during anomaly months of the second principal component (PC2) of monthly accumulated precipitation anomalies in March, April and May in Scandinavia 1981 to 2014. Statistically significant anomalies at the 90 % level are encircled by black lines. The NDVI anomalies are based on monthly averages of NDVI in June, July and August respectively in Scandinavia 1981 to 2014.

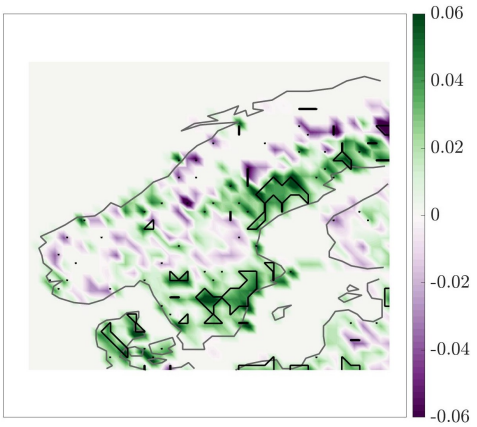

(a) Mean monthly summer NDVI anomalies during positive PC3 anomaly months

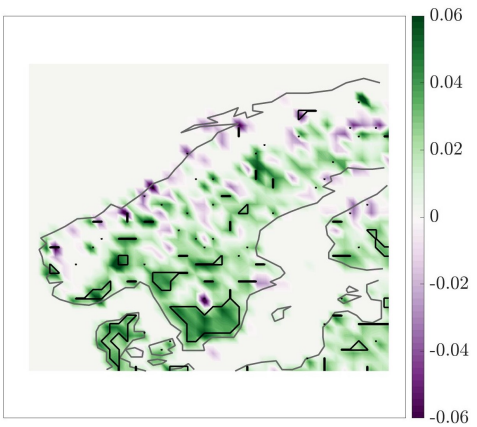

(b) Mean monthly summer NDVI anomalies during negative PC3 anomaly months.

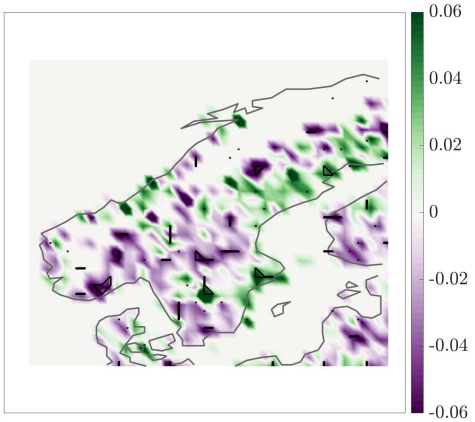

(c) The difference in mean monthly summer NDVI anomalies between positive and negative PC3 anomaly months.

Figure IX: Mean monthly summer NDVI anomalies during anomaly months of the third principal component (PC3) of monthly accumulated precipitation anomalies in March, April and May in Scandinavia 1981 to 2014. Statistically significant anomalies at the 90 % level are encircled by black lines. The NDVI anomalies are based on monthly averages of NDVI in June, July and August respectively in Scandinavia 1981 to 2014.

A.7 North's rule of thumb based on monthly summer precipitation anomalies

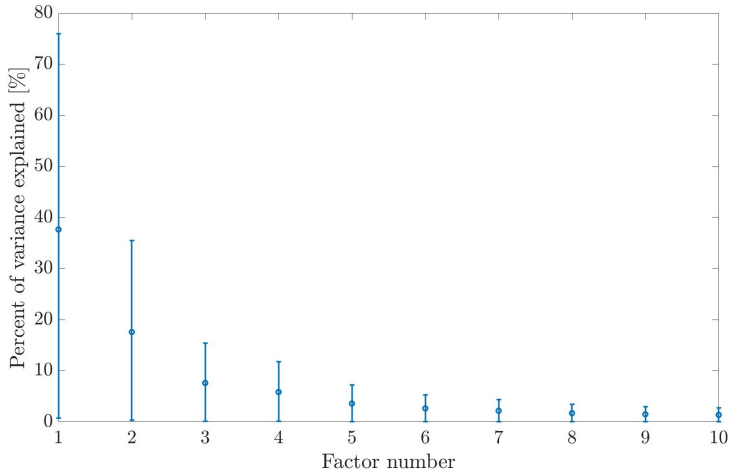

Figure X: The percent of variance explained by the first ten eigenvalues of mean monthly summer precipitation anomalies, with the associated sampling errors. The three first eigenvalues were determined to be distinct through the application of North's rule of thumb (North et al. 1982).

A.8 Spatial pattern of the EOFs based on monthly summer precipitation anomalies

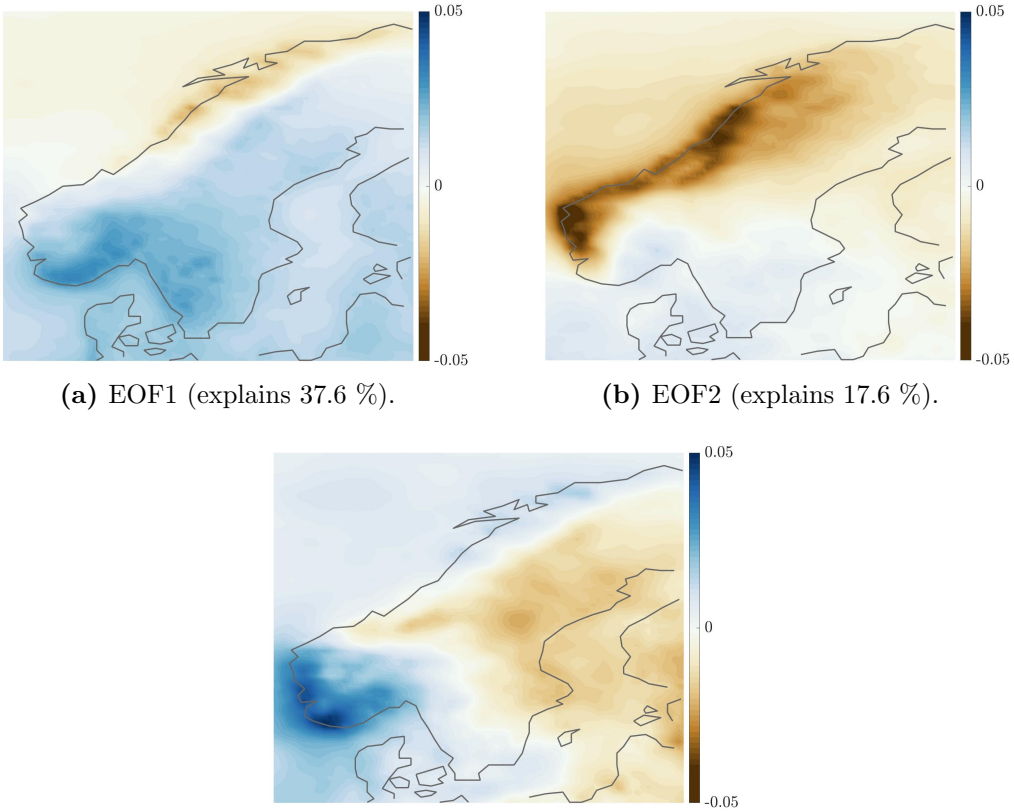

(a) EOF1 (explains 37.6 %).

(b) EOF2 (explains 17.6 %).

(c) EOF3 (explains 7.61 %).

Figure XI: Spatial patterns of the first three empirical orthogonal functions (EOFs) chosen for analysis. The spatial patterns show the variability of mean monthly summer precipitation, based on cumulative precipitation in June, July and August in Scandinavia 1981 to 2014. The colorbar shows the precipitation anomalies in mm/month.

A.9 Principal components based on monthly summer precipitation anomalies

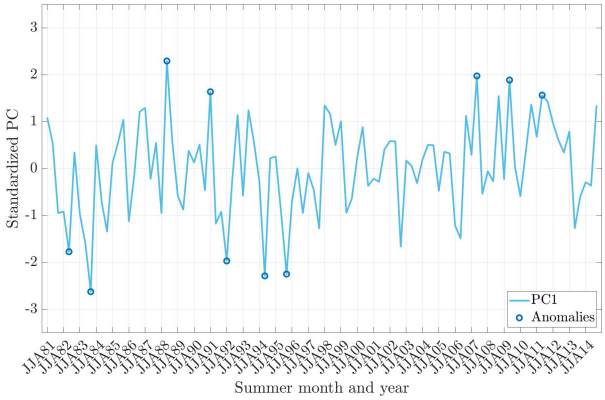

(a) Standardized PC1.

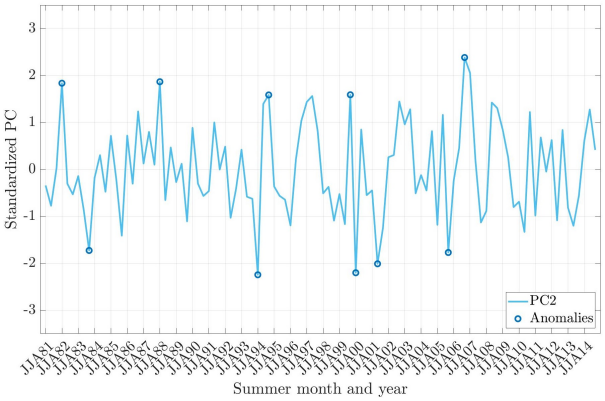

(b) Standardized PC2.

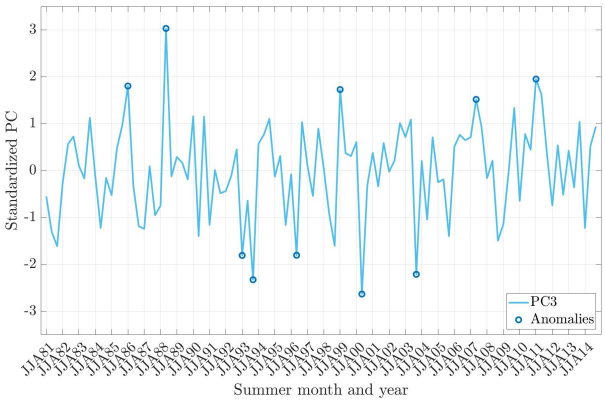

(c) Standardized PC3.

Figure XII: Standardized principal components (PCs) corresponding to the first three empirical orthogonal functions (EOFs) of monthly summer precipitation anomalies. The mean anomalies are based on the cumulative precipitation in June, July and August in Scandinavia 1981 to 2014. The ticks of the x-axis lie on the point of June each year, thus the two points in the graph following each x-axis tick are July and August each year. For each PC the five largest and the five lowest values are marked, showing months of anomalous precipitation variability.

A.10 Monthly summer NDVI anomalies for the principal components of monthly summer precipitation anomalies

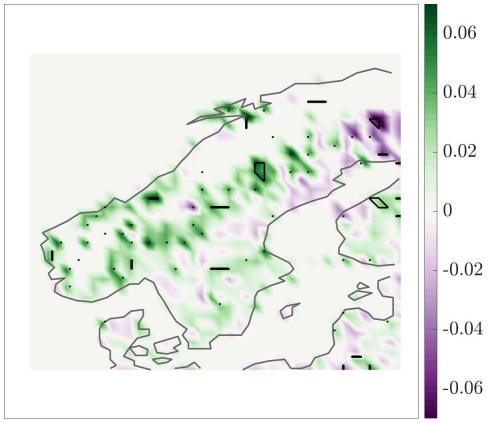

(a) Mean monthly summer NDVI anomalies during positive PC1 anomaly months.

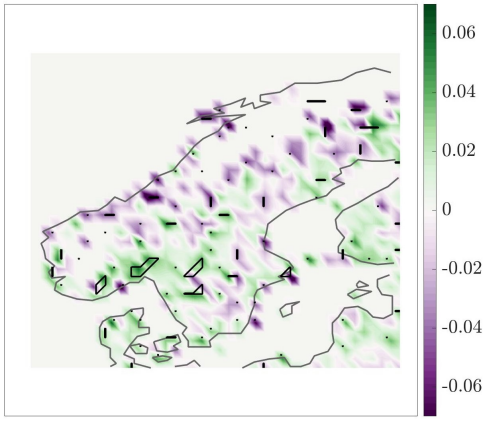

(b) Mean monthly summer NDVI anomalies during negative PC1 anomaly months.

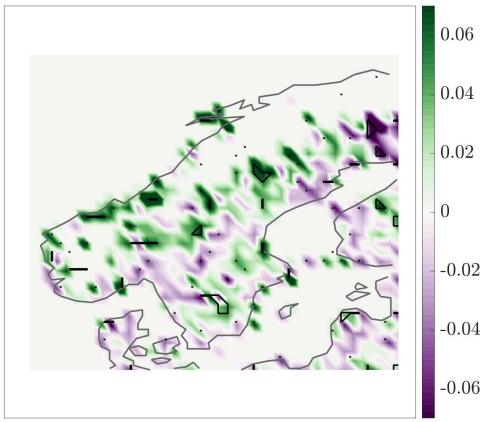

(c) The difference in mean monthly summer NDVI anomalies between positive and negative PC1 anomaly months.

Figure XIII: Mean monthly summer NDVI anomalies during anomaly months of the first principal component (PC1) of monthly accumulated precipitation anomalies in June, July and August in Scandinavia 1981 to 2014. Statistically significant anomalies at the 90 % level are encircled by black lines. The NDVI anomalies are based on monthly averages of NDVI in June, July and August respectively in Scandinavia 1981 to 2014.

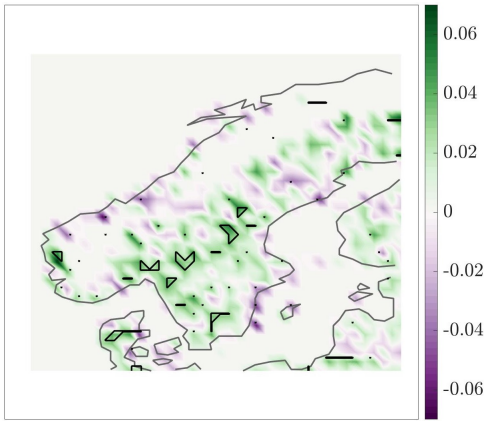

(a) Mean monthly summer NDVI anomalies during positive PC2 anomaly months.

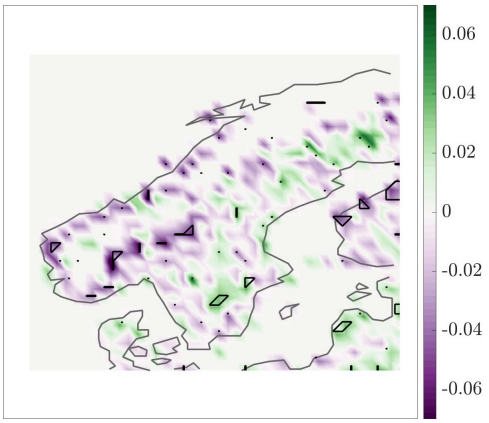

(b) Mean monthly summer NDVI anomalies during negative PC2 anomaly months.

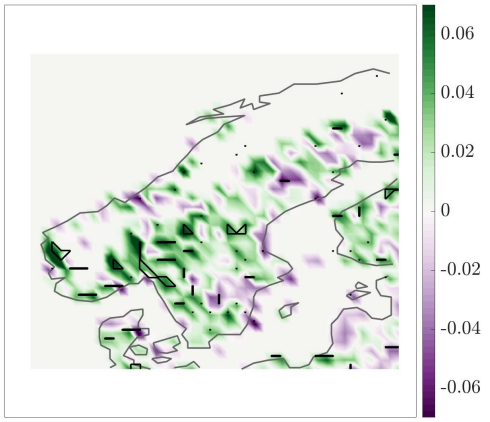

(c) The difference in mean monthly summer NDVI anomalies between positive and negative PC2 anomaly months.

Figure XIV: Mean monthly summer NDVI anomalies during anomaly months of the second principal component (PC2) of monthly accumulated precipitation anomalies in June, July and August in Scandinavia 1981 to 2014. Statistically significant anomalies at the 90 % level are encircled by black lines. The NDVI anomalies are based on monthly averages of NDVI in June, July and August respectively in Scandinavia 1981 to 2014

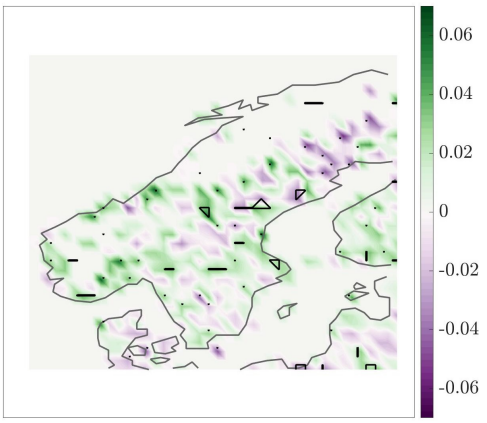

(a) Mean monthly summer NDVI anomalies during positive PC3 anomaly months.

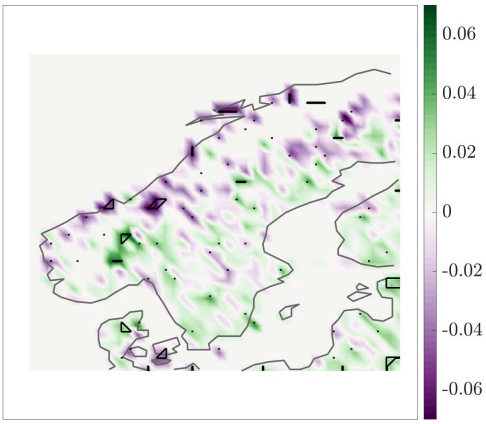

(b) Mean monthly summer NDVI anomalies during negative PC3 anomaly months.

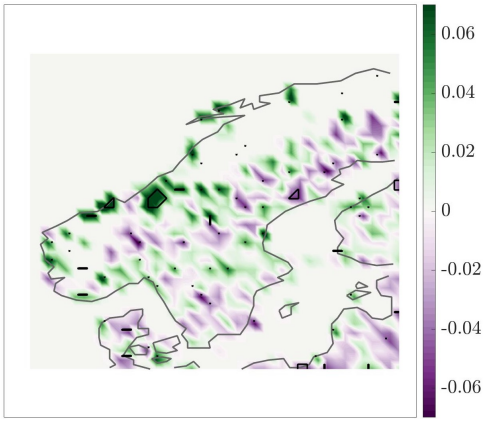

(c) The difference in mean monthly summer NDVI anomalies between positive and negative PC3 anomaly months.

Figure XV: Mean monthly summer NDVI anomalies during anomaly months of the third principal component (PC3) of monthly accumulated precipitation anomalies in June, July and August in Scandinavia 1981 to 2014. Statistically significant anomalies at the 90 % level are encircled by black lines. The NDVI anomalies are based on monthly averages of NDVI in June, July and August respectively in Scandinavia 1981 to 2014